

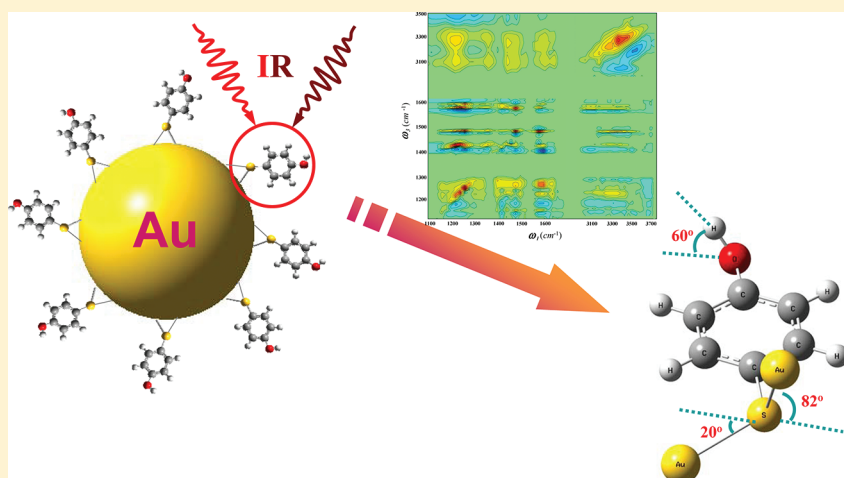
Molecular Conformations and Dynamics on Surfaces of Gold Nanoparticles Probed with Multiple-Mode Multiple-Dimensional Infrared Spectroscopy

Hongtao Bian,[†] Jiebo Li,[†] Hailong Chen,[†] Kaijun Yuan,[†] Xiewen Wen,[†] Yaqin Li,[‡] Zhigang Sun,[‡] and Junrong Zheng^{*,†}

[†]Department of Chemistry, Rice University, Houston, Texas 77005, United States

[‡]State Key Laboratory of Molecular Reaction Dynamics, Dalian Institute of Chemical Physics, Chinese Academy of Sciences, Dalian 116023, Liaoning, People's Republic of China

 Supporting Information



ABSTRACT: Knowledge about molecular conformations and nuclear and electronic motions on surfaces of metal nanomaterials is critical for many applications but extremely difficult to obtain. We demonstrate that valuable information of this sort can be determined using multiple-mode multiple-dimensional vibrational spectroscopy. A model compound, 4-mercaptophenol, on the surface of 3.5 nm gold nanoparticles demonstrates the method. Its 3D molecular conformations and vibrational dynamics on the particle surfaces were determined with the method. The experimental results imply that on the particle surfaces, the ligand molecules cannot form energy-optimized hydrogen bonds because of the surface geometry constraint. The conclusion is supported with experiments on the ligand molecules in the crystalline phase and in a dilute solution. Our experiments also showed that the effect of the particle surface nonadiabatic electron/vibration coupling does not play a significant role in the vibrational relaxation of high-frequency modes ($>1000\text{ cm}^{-1}$) about 3 Å away from the surface. Simple theoretical calculations support this observation. The method holds promise as a general tool for the studies of molecular structures and dynamics on the surfaces of nanomaterials. The capability of resolving 3D molecular conformations on nanomaterials surfaces is expected to be helpful for understanding specific intermolecular interactions and conformation-selective reactions (e.g., chirality selectivity) on the surfaces of these materials.

1. INTRODUCTION

Metallic nanoparticles have been intensively investigated over the past three decades for a very wide range of applications from catalysis, to biological processes, to nanophotoelectronics,^{1–4} for example, Au nanoparticles coated with functionalized ligands as candidates for catalysts of selective chemical reactions, drug delivery, protein labeling, cancer treatments, and specific molecular recognition processes.^{5–8} On the surfaces of these nanoparticles, molecular conformations and energy dynamics of adsorbed molecules play a crucial role

in determining the yield and the selectivity of products, for example, chirality selectivity, of a surface reaction, the effects of thermal therapeutic applications, and the outcomes of molecular recognitions.^{6,9,10} However, in general, such molecular information is difficult to be determined by traditional methods, for example, X-ray diffraction (XRD),

Received: January 31, 2012

Revised: March 9, 2012

Published: March 16, 2012



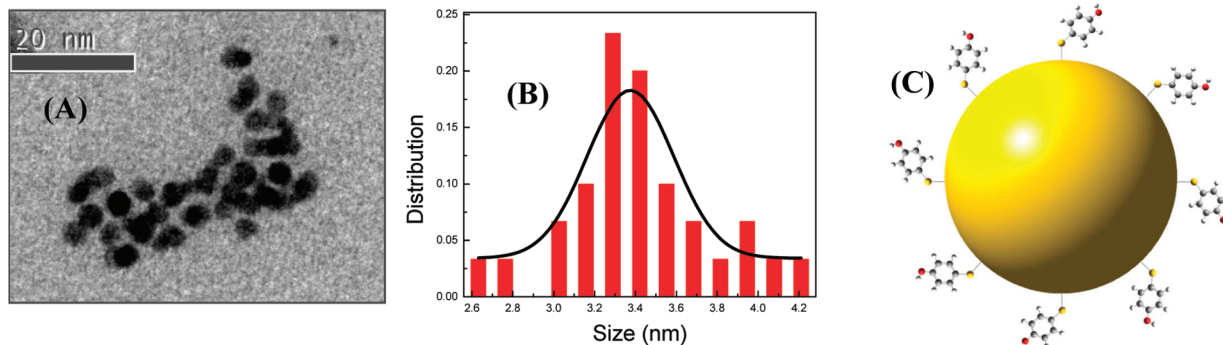


Figure 1. (A) TEM image of ~ 3.5 nm gold particles. (B) Size distribution of the nanoparticles from TEM results. (C) Schematic representation of 4-mercaptophenol on the Au particles. The molecule/particle ratio is the actual ratio. On the surface, not indicated on the figure, the OH groups are actually H-bonded to each other as evident in the FTIR measurements. In addition, the actual molecular distribution on the surface is unknown.

because of the spatial or temporal resolution problem or the crystallization issue, or NMR, because of the electronic/charge properties of the particle metal atoms, which typically shift the NMR peak positions and broaden peak lineshapes,¹¹ or predicted by calculations because of the difficulty of precisely incorporating the surface atomic information into the calculations. In this work, we demonstrate that valuable information of this sort can be determined using multiple-mode multiple-dimensional vibrational spectroscopy.¹²

A model system, 3.5 nm gold nanoparticles coated with 4-mercaptophenol (*p*-HO-C₆H₄-SH), was used for this study. The molecule, 4-mercaptophenol, can form a surface monolayer through strong S–Au bonds with the particle substrate. This system is a prototype of molecular electronics in that this molecule has been considered as one of the best candidates for connecting a molecular wire to an electrode.¹³ Almost any functional group can be connected to this molecule through reactions with the hydroxyl group, and its delocalized π -electrons on the benzene ring were suspected to be able to interact directly with the electrode surface electrons. Such a direct interaction was expected to facilitate the electronic transportation and the relaxation of heat of the molecular wire induced by the electronic motions on the molecular junction. So far, no experimental data are available to directly test these hypotheses at the molecular level, mainly because of the lack of information about the surface molecular conformations and the couplings between surface electrons of the metal and the motions of the molecular nuclei. Here, using the multiple-mode multiple-dimensional vibrational spectroscopic technique, we are able to obtain information about the three-dimensional molecular conformation and nuclear motion dynamics of 4-mercaptophenol on the surface of the 3.5 nm Au nanoparticles. We found that about 3 Å away from the surface, the Born–Oppenheimer approximation (BOA) holds for the surface molecular vibrations with fundamental frequencies higher than 900 cm^{-1} , and the calculated energy-optimized ligand molecular conformations without precise knowledge about the particle surface structures are different from the most probable conformations experimentally obtained. The surface conformations are substantially different from those in the ligand crystal or a dilute CCl₄ solution.

2. EXPERIMENTS

The optical setup has been described previously.^{14–17} In summary, a ps amplifier and a fs amplifier are synchronized with the same seed pulse. The ps amplifier pumps an OPA to

produce 0.7–1 ps mid-IR pulses with a bandwidth 10–30 cm^{-1} in a tunable frequency range from 400 to 4000 cm^{-1} with energy 1–40 $\mu\text{J}/\text{pulse}$ at 1 kHz. The fs amplifier pumps another OPA to produce \sim 140 fs mid-IR pulses with a bandwidth \sim 200 cm^{-1} in a tunable frequency range from 400 to 4000 cm^{-1} at 1 kHz. In the multiple dimensional scanning experiments, the ps IR pulse is the pump beam (the pump power is adjusted based on need, and the interaction spot varies from 100 to 500 μm). The fs IR pulse is the probe beam, which is frequency resolved by a spectrograph (resolution is 1–3 cm^{-1} dependent on the frequency) yielding the probe frequency axis of a multiple-dimensional spectrum. Scanning the pump frequency yields the other frequency axis of the spectrum. Scanning the delay between the pump and the probe provides the time axis. Two polarizers are placed in the probe beam path to selectively measure the parallel or perpendicular polarized probe signal relative to the pump beam. Vibrational lifetimes are obtained from the rotation-free 1–2 transition signal $P_{\text{life}} = P_{\parallel} + 2 \times P_{\perp}$, where P_{\parallel} and P_{\perp} are parallel and perpendicular data, respectively. Rotational relaxation times are acquired from $\tau = (P_{\parallel} - P_{\perp})/(P_{\parallel} + 2 \times P_{\perp})$. The whole setup including frequency tuning is computer controlled.

The chemicals were purchased from Aldrich and used as received. The synthesis of Au nanoparticles was based on the literature.¹⁸ Specifically, 10 mL of 6.6 mM HAuCl₄ aqueous solution was added into 10 mL of 48 mM 4-mercaptophenol methanol solution. The mixture was allowed to stand for 1 h at room temperature. Ten milliliters of 10 mM NaBH₄ solution was then added dropwisely into the ice bath-cooled mixture. After 4 h at room temperature, the precipitated product was collected and purified by rinsing with ethanol and subsequent centrifuging for three times. The resulting Au nanoparticles were characterized with transmission electron microscopy (TEM) and Fourier transform infrared (FTIR). Samples for the FTIR and 2D IR measurements were contained in sample cells composed of two CaF₂ windows separated by a Teflon spacer. The thickness of the spacer was adjusted depending upon the optical densities of different modes from 2.5 to 205 μm . The experimental optical path and apparatus after the generation of mid-IR pulses was purged with CO₂- and H₂O-free clean air. All of the measurements were carried out at room temperature (22 °C). The 4-mercaptophenol in CCl₄ solution is 0.25 wt %. The nanoparticle samples in all measurements are solid powder.

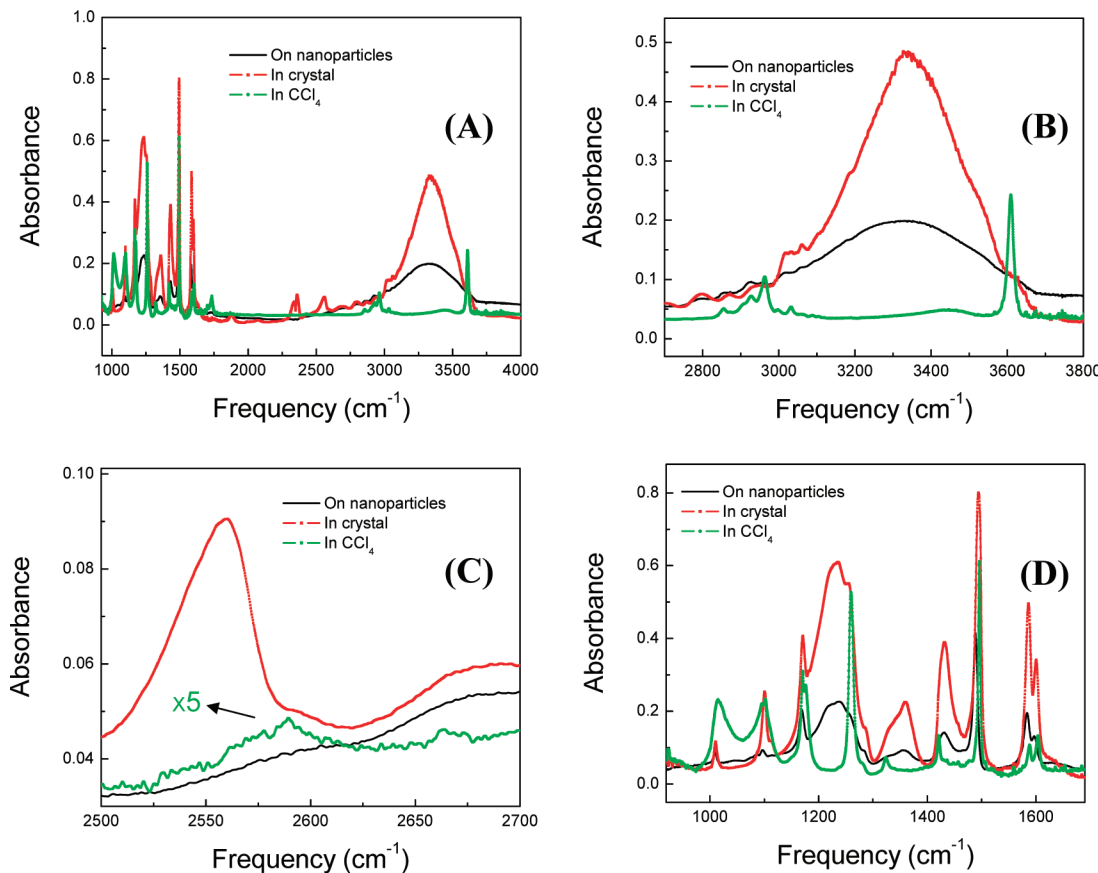


Figure 2. FTIR spectra of 4-mercaptophenol in a CCl_4 solution, in pure crystal, and on the Au nanoparticle surface in different frequency ranges: (A) 900–4000 cm^{-1} ; (B) 2700–3800 cm^{-1} for the hydrogen-bonded and free O–H stretches; (C) 2500–2700 cm^{-1} for the S–H stretches; and (D) 900–1700 cm^{-1} for the C=C stretches ($\sim 1590 \text{ cm}^{-1}$), C–O stretch ($\sim 1240 \text{ cm}^{-1}$), C–H bending and rocking ($\sim 1096, 1488, 1430$, and 1356 cm^{-1}), and O–H bending ($\sim 1170 \text{ cm}^{-1}$). Assignments are based on DFT calculations.

Structures were calculated with density functional theory (DFT) computations using Gaussian 09. Several levels and basis sets were used to compare the calculation results.

3. RESULTS AND DISCUSSION

3.1. Particle Size and FTIR. Figure 1 displays the TEM image and schematic representation of the coated gold nanoparticles. The particle size is $\sim 3.5 \text{ nm}$ with a relative narrow distribution. Figure 2 displays the FTIR spectra of the 4-mercaptophenol-coated Au nanoparticles, 4-mercaptophenol in CCl_4 (0.25 wt %), and 4-mercaptophenol in its pure crystal. The spectra reveal a few structural features about the 4-mercaptophenol molecular layer on the particle surface. First, the OH groups of most surface molecules form hydrogen bonds with each other, as evident by the broad OH stretch peak (3000 – 3600 cm^{-1}) in Figure 2B. As a contrast, in a dilute CCl_4 solution, 4-mercaptophenol can not form hydrogen bonds, resulting in a very sharp OH stretch peak at $\sim 3610 \text{ cm}^{-1}$. These two types of OH stretches are frequently observed in alcohol/ CCl_4 solutions.^{19,20} In the crystal or on the surface of nanoparticles, the sharp free OH stretch peak almost completely disappears. Only the broad band exists. The results indicate that in the two latter cases, most of the OH groups form hydrogen bonds. Another feature that the FTIR spectra reveal is the formation of Au–S bond between the 4-mercaptophenol molecules and the Au nanoparticles. As shown in Figure 2C, the S–H stretch vibrational peaks (2550 – 2600 cm^{-1}) are evident in the crystal or in the CCl_4

solution. However, these peaks are hardly visible on the nanoparticle surface, indicating that most of the S–H groups have reacted with the gold nanoparticles to form the Au–S bonds. In Figure 2C, the S–H stretch peak of the crystal sample is much stronger than that of the CCl_4 solution because the S–H groups form hydrogen bonds with adjacent molecules in the crystal. The hydrogen bond increases the S–H stretch transition dipole moment for several times and shifts the peak to a lower frequency. A similar increase was also observed by us when a thiol molecule was dissolved in CH_3CN to form a hydrogen bond of S–H···N≡C. Figure 2D displays the FTIR spectra in the frequency range between 900 to 1700 cm^{-1} where the C=C stretches ($\sim 1590 \text{ cm}^{-1}$), C–O stretch ($\sim 1240 \text{ cm}^{-1}$), and C–H bending and rocking and O–H bending ($\sim 1096, 1170, 1488, 1430$, and 1356 cm^{-1}) reside. The FTIR spectra of the crystal sample and the particle sample are very similar in this frequency range probably because of the H-bonds and the close-packed nature of the molecules in both cases,¹⁸ different from that in the CCl_4 solution. However, the similarity or difference of the FTIR spectra does not imply the same similarity or difference of molecular conformations in the three samples. As we can see from the 2D IR results introduced in the following, the molecular conformations of 4-mercaptophenol on the particle surface are actually very different from those in the crystal in which the molecules adopt very similar conformations to those of isolated molecules in the dilute CCl_4 solution.

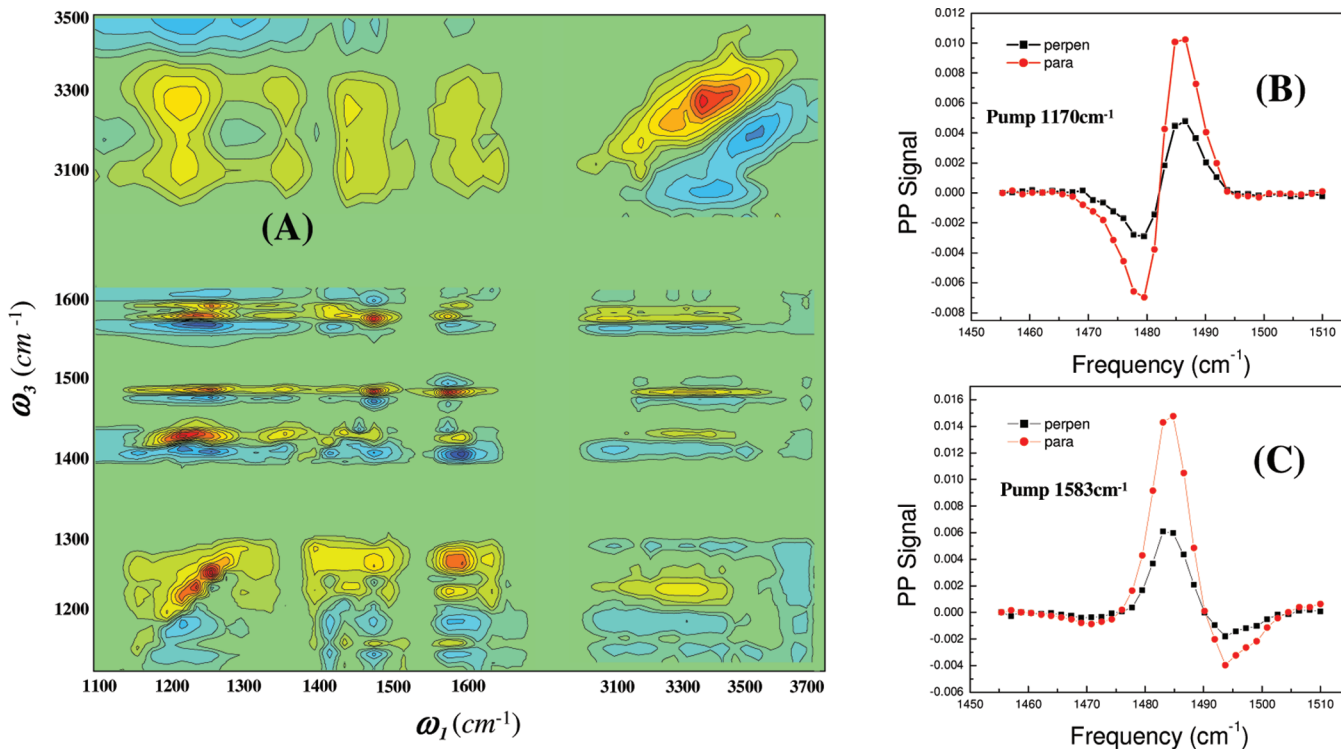


Figure 3. (A) 2D spectra of 4-mercaptophenol on the surfaces of 3.5 nm Au nanoparticles in two different frequency ranges. The relative intensities of peaks are adjusted to be comparable. Detailed factors are provided in the Supporting Information. (B and C) Two color pump/probe data probed at the frequency range of one C–H bending mode by pumping different modes. Different polarization-selective intensity ratios I_{\parallel}/I_{\perp} represent different vibrational cross-angles between the C–H bending mode and the different pumped modes. In the spectrum, the peaks between 1400–1600 cm^{-1} look rounder. This is mainly because the peaks in this frequency range are narrower, while the bandwidth of our pump laser is relatively constant along the frequency. Therefore, the undeconvoluted peaks appear rounder for narrower peaks.

3.2. Multiple-Mode 2D IR Spectra. The FTIR spectra in Figure 2 indicate that on the surfaces of Au nanoparticles, most of the OH groups form hydrogen bonds, and most of the S–H stretch intensity disappears probably because of the formation of Au–S bonds. Further structural information about the conformations of surface molecules is difficult to obtain from such measurements. In principle, whenever the molecular conformation of a molecule changes, some of its normal modes will inevitably change their vibrational frequencies, which can be detected with FTIR. However, Fermi resonances, which ubiquitously exist in molecular vibrations, can also affect the vibrational frequencies.^{21,22} The vibrational frequency changes induced by these two sources cannot be experimentally resolved with FTIR. Therefore, it is almost impossible to determine molecular conformations solely based on the vibrational frequencies.

Fermi resonances originate from the anharmonic nature of molecular vibrations. A combination band or an overtone whose origin is in general unknown with a very small transition dipole moment (this is why it is also called “dark mode”) can be anharmonically coupled to a normal mode of the same symmetry and a similar frequency (energy) with a much bigger transition dipole moment (called “bright mode”). The vibrational coupling results in two consequences: (1) the high frequency mode shifts to higher energy and the low energy mode shifts to still lower energy; (2) the dark mode gains intensity and the bright mode decreases in intensity. This type of Fermi resonances can not only significantly change vibrational frequencies but also produce many additional peaks in FTIR spectra, which make peak assignments very

difficult. This is one major difficulty and pitfall of applying FTIR in determining molecular structures and properties.

Our method for determining molecular conformations does not rely on the detailed values of vibrational frequencies.¹² It measures the angle between the transition electric dipoles of two vibrations.¹² The experimentally measured vibrational angles are sensitive to the molecular conformation because a conformation change (atomic coordinate change) inevitably causes the directions of transition electric dipoles of vibrations to change.¹² These angles are in general not sensitive to Fermi resonances because the dipole transition moment of a dark mode is in general less than a few percent of that of a bright mode.²³ The experimental signal for determining vibrational transition dipole direction of a peak induced by Fermi resonance is therefore mainly aligned with the bright mode transition. The dark mode can at most change the direction of the signal 1 or 2°, which is within our experimental uncertainty. A mathematical analysis is provided in the Supporting Information.

The way of determining molecular conformations on the nanoparticle surface presented here is similar to that used to determine molecular conformations in liquids.¹² Both measure the cross-angle between the 0–1 transition dipole moment vectors of any two normal modes. By mapping the cross-angles among a sufficiently big number of normal modes that cover the complete molecular space, the 3D molecular conformations can then be constructed by translating the measured vibrational angles among these modes into the cross-angles among the chemical bonds with suitable theoretical tools. More angles

measured in general will provide more structural constraints and yield more precise molecular conformations.

The principle of the method has been described in detail in our previous publication.¹² Briefly, when two vibrational modes are anharmonically coupled, the excitation of one mode will affect the vibrational frequency of the other.^{15,24–38} In most cases, it will shift the vibration of the other mode to a lower frequency (e.g., Figure 3B). In fewer cases, it can shift the vibration of the other mode to a higher frequency (e.g., Figure 3C).³⁹ The vibrational excitation-induced frequency shifts produce off-diagonal peak pairs in the 2D IR spectra (Figure 3A). These off-diagonal peak pairs are called combination band peaks. Their signal comes from the simultaneous excitations of both coupled modes. Because the two coupled modes have a cross-angle θ between their transition dipole moment vectors, very qualitatively speaking, the combination band signal will be maximized if the cross-angle between the polarizations of the two excitational lasers is the same as θ . If the sample is isotropically distributed, θ can be quantitatively determined by experiments with two sets of different pump/probe relative polarizations, parallel and perpendicular, through the following equation:

$$\frac{I_{\perp}}{I_{\parallel}} = \frac{2 - \cos^2 \theta}{1 + 2 \cos^2 \theta} \quad (1)$$

where I_{\parallel} and I_{\perp} are peak intensities from experiments with parallel and perpendicular pump/probe polarizations, respectively.

Figure 3 display the multiple-mode 2D IR spectra of 4-mercaptophenol on the surfaces of 3.5 nm Au nanoparticles covering the O–H stretch and bending, C=C stretches, the C–O stretch, and the C–H stretches and bendings. The cross-peak intensities for parallel and perpendicular polarizations of the pump and probe for three pairs of combination bands of C–H bending/O–H bending, and C–H bending/C=C stretch are also shown in Figure 3 (others are listed in the Supporting Information). The polarization-selective intensities of 16 pairs of cross-peaks are then plugged into eq 1 to obtain the vibrational cross-angle θ . We then use DFT calculations to translate these vibrational angles into relative bond angles of the molecule to obtain molecular conformation.

3.3. Vibrational Dynamics on the Nanoparticle Surface. The current method we use to translate vibrational angles into bond angles is to preset a series of molecular conformations and calculate their vibrational cross-angles and compare the calculated angles to the experimentally measured angles until a minimum was found. The method has worked well for relatively small molecules in liquids,¹² but it cannot be immediately applied to the coated Au nanoparticle system. The main reason is that it is too time-consuming to reliably calculate the 3.5 nm gold nanoparticles. A way to bypass this difficulty could be to reduce the number of gold atoms in the calculations if the vibrational properties of the surface molecules are not significantly affected by the surface electrons of the gold particles. However, this approach can fail if the assumption it is based on is invalid.

According to literature, 3.5 nm Au nanoparticles are already metallic.^{40–44} There have been accumulating evidence from molecular beam experiments, IR line shape analysis, and pump/probe experiments^{45–52} that on some clean metal surfaces the metal surface electrons can be strongly coupled to the vibrations of the surface molecules, which leads to the

breakdown of the BOA. It is conceivable that a similar mechanism can also occur on surfaces of metallic nanoparticles. In a metal, the surface electronic states form a continuum of electronic states. The electron–hole pair transitions between electronic levels in the conduction band can be strongly coupled to the nuclear motions of an adsorbate molecule and provide a mechanism for energy relaxation from an adsorbate molecule. This mechanism even calls into question the applicability of the concept of motion evolving on a potential energy surface. Metal nanoparticles can be metallic (big size) or an insulator (small size).⁴⁴ Their surface electrons can have a near continuum of states or discrete energy levels.⁴³ If the nanoparticle is sufficiently small, it is not metallic any more. It is possible that reducing the number of Au atoms in the calculations of converting the experimental vibrational angles into bond angles can miss the effect of the nonadiabatic electron/vibrational coupling. However, if the nonadiabatic electron/vibrational couplings are much weaker as compared to the intramolecular vibrational couplings, it is then acceptable not to consider the nonadiabatic electron/vibrational couplings in the calculations.

Simple inspections on the FTIR spectra of the crystalline sample and the nanoparticle sample reveal no obvious peak intensity ratio changes in the nanoparticle sample, indirectly indicating that the surface electrons do not have apparent effects on the intramolecular vibrations. The result also implies that the surface plasmon (if any) does not enhance the IR signal for a significant amount, because the surface plasmon preferably enhances the electric field along the surface normal. In the surface molecules, some of the vibrational modes can be aligned parallel to the surface normal. Some can be perpendicular to the surface normal. If the surface plasmon does enhance the IR electric field significantly, we would have observed some apparent peak intensity ratio changes in the FTIR spectrum.

To more quantitatively compare the nonadiabatic electron/vibrational couplings and the intramolecular vibrational couplings and possible intermolecular vibrational couplings, we measured the vibrational lifetimes (the first vibrational excited state) of the O–H stretch, the O–H bending, the C=C stretch, the C–H bending, and the C–O stretch on the 3.5 nm Au nanoparticle surface, in the pure 4-mercaptophenol crystal and in a 4-mercaptophenol/CCl₄ solution. Results are shown in Table 1. Except for the C–O stretch with the same, but substantially shortened (probably because of a Fermi resonance), lifetimes in the crystal and on the surface, the vibrational relaxations of those major vibrational modes of 4-mercaptophenol are actually the same for the three different

Table 1. Vibrational Lifetimes of Major Vibrational Modes of 4-Mercaptophenol in Different Environments

vibrational mode	nano particles (ps)	crystal (ps)	in CCl ₄ (ps)
O–H stretch (3340 cm ⁻¹)	1.4 ± 0.3	1.8 ± 0.3	1.5 ± 0.2
C=C stretch (1584 cm ⁻¹)	4.2 ± 0.6	4.6 ± 0.6	4.2 ± 0.3
C–H bending (1488 cm ⁻¹)	2.6 ± 0.4	2.7 ± 0.4	2.4 ± 0.3
C–O stretch ^a (1237 cm ⁻¹)	1.0 ± 0.2	1.0 ± 0.2	4.0 ± 0.2
O–H bending (1169 cm ⁻¹)	1.3 ± 0.2	1.0 ± 0.2	1.4 ± 0.2

^aIn CCl₄ solution, the central peak frequency is at 1280 cm⁻¹. In crystal and on nanoparticles, the frequency is at 1237 cm⁻¹. It is conceivable that the redshift is caused by an accidental degeneracy, which also shortens the lifetime.

cases: on the particle surface, in molecular crystal, and in CCl_4 . The results indicate that intramolecular relaxations dominate. The solvent effect or the surface nonadiabatic electron/vibration couplings are minor factors in terms of affecting the relaxation of these high frequency vibrations. [Note that the lifetime of the O–H stretch in the CCl_4 solution measured is for the H-bonded species. It is well-known that the H-bonds can significantly reduce the vibrational lifetime of the O–H stretch (from tens of ps to a few ps).^{20,53}] For this mode, the intermolecular vibrational coupling (H-bonding) is bigger than the intramolecular coupling, or the intramolecular coupling is significantly modified by H-bonding.¹⁴] These results suggest that it is probably acceptable to omit the surface nonadiabatic electron/vibration couplings in calculations to obtain the molecular conformations of 4-mercaptophenol on surfaces of the 3.5 nm Au nanoparticles.

These results differ from the case of CO absorbed on metal surfaces where the nonadiabatic electron/vibration coupling dominates.^{49–52} The direct chemical bond between the CO and the surface is the highly probable reason for the strong nonadiabatic electron/vibration coupling. In our system, because of the existence of Au–S–C bonds, all of the vibrational modes investigated are at least 3 Å away from the surface. Such a distance can dramatically reduce the non-adiabatic electron/vibration coupling. To more quantitatively analyze the experimental results, we used theory to calculate the vibrational relaxation rates induced by the nonadiabatic electron/vibration coupling.⁵⁴ The vibrational mode of 4-mercaptophenol can be considered as a polarizable point dipole, which is located at a distance of d from the surface of the gold nanoparticle. According to the linear-response theory and Fermi's golden rule, for a spherically symmetric particle, the energy transfer rate can be derived as (in Rydberg atomic units):⁵⁴

$$k = 4\mu^2 \sum_{l=1}^{\infty} \frac{\text{Im } \alpha_l(\omega)}{(R + d)^{2(l+2)}} [(l+1)^2 \cos^2 \theta + P'_l(x)|_{x=1} \sin^2 \theta] \quad (2)$$

where μ is the transition dipole moment, R is the radius of the nanoparticle, θ represents the angle between the dipolar axis and the line connecting the point dipole with the center of the sphere, P'_l is the derivative of the l -th Legendre polynomial P_l , and $\alpha_l(\omega)$ is the l -pole polarizability of the metallic sphere.

By using the Drude-like dielectric constant $\epsilon(\omega)$, the l -pole polarizability can be written as

$$\alpha_l(\omega) = \frac{\epsilon(\omega) - 1}{\epsilon(\omega) + (l+1)/l} R^{2l+1} \quad (3)$$

with⁵⁵

$$\epsilon(\omega) = 1 - \omega_p^2 / [\omega^2 + i\omega(\gamma_\infty + v_f/R)] \quad (4)$$

where ω_p is the plasma frequency and v_f is the Fermi velocity of the electrons in the metal bulk. For gold, we have $\omega_p = 8.55$ eV, $\gamma_\infty = 0.0184$ eV, and $v_f = 1.4 \times 10^6$ m/s.⁵⁶ With these parameters and the diameter of nanoparticle $D = 2R = 3.5$ nm, the energy transfer rate for the major vibrational modes of 4-mercaptophenol can be calculated. Calculated results are shown in Table 2.

It can be seen that energy transfer rates (Table 2) from the adsorbate (coated) molecules to the gold nanoparticle induced

Table 2. Calculated Energy Transfer Rates for Major Vibrational Modes of 4-Mercaptophenol

vibrational mode	μ (Debye)	angle (degree)	distance (Å)	$1/k$ (ps)	$1/k^a$ (ps)
3340 cm ⁻¹	0.28	27.7	7.1	167	265
1584 cm ⁻¹	0.13	22.9	4.5	337	322
1488 cm ⁻¹	0.20	37.6	4.5	229	145
1237 cm ⁻¹	0.47	22.0	5.8	80	104
1169 cm ⁻¹	0.29	27.0	7.1	451	718

^aThe rates calculated from the flat metal surface model.

by the nonadiabatic electron/vibration coupling mechanism are about 2 orders of magnitude smaller than the decay rates observed in our experiments (Table 1). This indicates that the surface nonadiabatic electron/vibration coupling is much smaller than the intramolecular vibrational coupling. The conclusion is further supported by calculations from eq 2 using various parameters. We notice that the energy transfer rate is dependent on various parameters, which are the angle between the dipolar axis and the line connecting the point dipole, the distance between the vibrational mode and the metal surface, and the size of the nanoparticle. To test the range of energy transfer rates by varying these parameters, we calculated the energy transfer rate dependences on these parameters, shown in Figure 4. The calculations show that, even under the conditions of a very close distance (e.g., 1.5 Å), or a smaller size of nanoparticle (e.g., 1 nm), the energy transfer rate induced by the nonadiabatic electron/vibration coupling is still a few times slower than the intramolecular relaxations.

The convergence of the series in eq 2 is mainly contributed by the item $R^{2l+1}/(R + d)^{2(l+2)}$. If the radius of the nanoparticle is too large as compared to the distance between the vibrational mode and the metal surface (i.e., $R \gg d$), it becomes $R^{2l+1}/(R + d)^{2(l+2)} \approx R^{-3}$, hence losing its convergence property. In this case, eq 2 will be no longer valid. However, if the size of nanoparticle is large enough, the molecule can be viewed as absorbed on a flat metal surface, and the flat metal surface model can be used to estimate the energy transfer rate.⁵⁷ The results are also listed in Table 2. It is clear that the energy transfer times obtained from these two methods are on the order of 100 ps or bigger, about 2 orders of magnitudes slower than that experimentally observed. The calculations are consistent with experimental observations. Both show that the vibrational dynamics of those modes of 4-mercaptophenol about 3 Å away from the gold nanoparticles are mainly dominated by the intramolecular energy transfer mechanism.

3.4. Molecular Conformations on the Surfaces of Au Nanoparticles. **3.4.1. Molecular Conformations of 4-Mercaptophenol in a Dilute CCl_4 Solution.** In the dilute CCl_4 solution, 4-mercaptophenol molecules are well separated from each other. The OH groups of most 4-mercaptophenol molecules do not form hydrogen bonds, manifested by the sharp OH stretch peak (3610 cm^{-1}) in Figure 2B. Similar to the phenol molecule,^{58–61} the OH group of 4-mercaptophenol of the most stable conformation is expected to be coplanar to the benzene ring because of the conjugation effect of the π -electrons. This is confirmed with DFT calculations in Figure 5A. The conformation can also be straightforwardly determined by our method.¹² By measuring the cross-angles among 16 pairs of its vibrational modes covering most of its molecular space in the solution, we found that in the most probable molecular

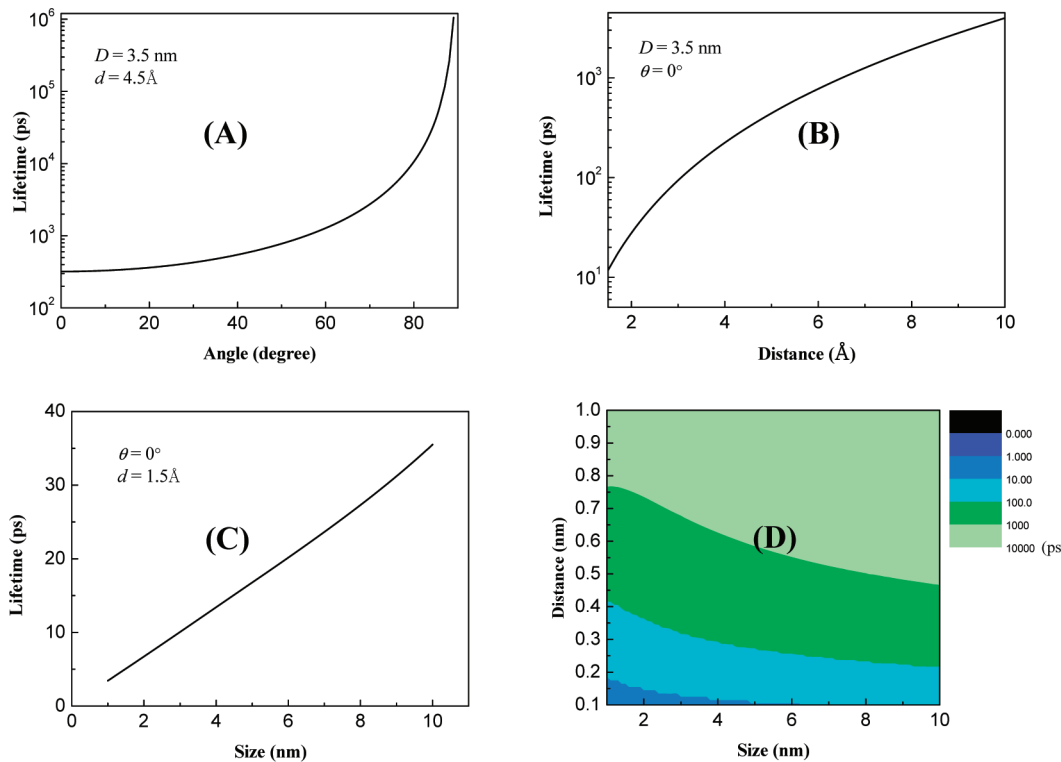


Figure 4. Calculated energy transfer time dependence on the (A) orientation of transition dipole moment θ , (B) distance between the vibrational mode and the metal surface d , (C) diameter of the nanoparticle D , and (D) both the distance and the particle size. All results are calculated using eqs 2–4, and μ is fixed at 0.2 D.

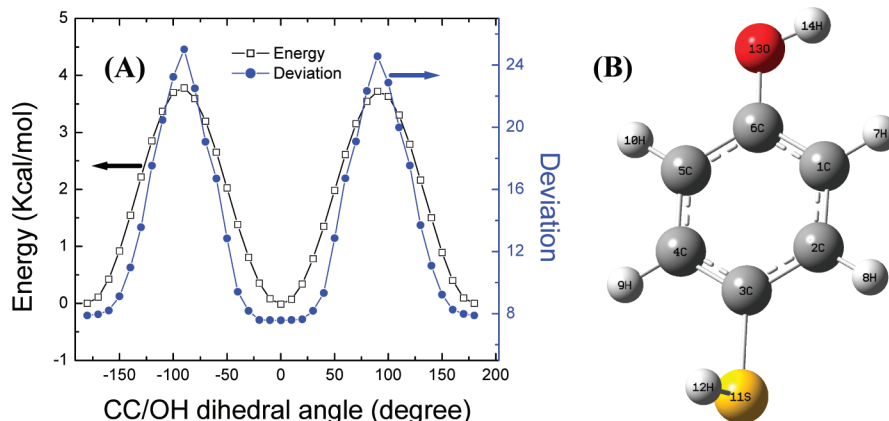


Figure 5. (A) Calculated potential energy surface of 4-mercaptophenol in CCl_4 (left axis) and the difference between calculated and experimental vibrational cross-angles Er vs the CC/OH dihedral angle $\text{C}(1)-\text{C}(6)/\text{O}(13)-\text{H}(14)$ (right axis), with a fixed dihedral angle of $\text{C}(4)-\text{C}(3)/\text{S}(11)-\text{H}(12)$ at -72° (the calculated optimal angle). (B) The calculated most stable conformation of 4-mercaptophenol in CCl_4 solution. The DFT calculations were performed using the CPCM model in CCl_4 with B3LYP/6-311++G(d,p).

conformation of 4-mercaptophenol, the OH group is indeed coplanar to the benzene ring (the Er curve in Figure 5A).

To determine molecular conformations, we first preset a series of molecular conformations based on the rotational degrees of freedom of the chemical bonds. DFT calculations are then performed on these conformations to obtain calculated vibrational cross-angles. Subsequently, the calculated angles are compared with experimental results. The conformation with calculated vibrational angles closest to those experimental values is considered as the most probable conformation

experimentally determined. The difference between experimental and calculated vibrational cross-angles is defined as Er :

$$Er = \frac{\sum_{i=1}^m |A_i^C - A_i^E|}{m} \quad (5)$$

where A_i^C is the calculated vibrational cross-angles of i -th pair of normal modes. A_i^E is the experimental value of the same pair. m is the number of the pairs, which is 16 for this liquid sample (detailed data are in the Supporting Information).

4-Mercaptophenol (shown in Figure 5B) can have many possible conformations by rotating O–H along its C–O bond and S–H along the C–S bond. Mapping its potential surface

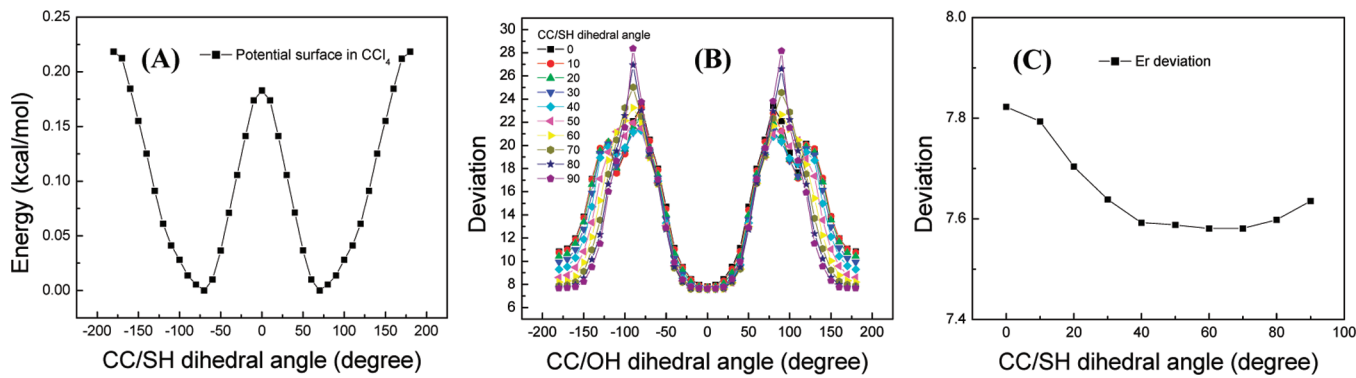


Figure 6. (A) Potential surface vs the $\text{C}(4)-\text{C}(3)/\text{S}(11)-\text{H}(12)$ dihedral angle at a fixed $\text{C}(1)-\text{C}(6)/\text{O}(13)-\text{H}(14)$ dihedral angle 0° . (B) Vibrational cross-angle difference Er vs the CC/OH dihedral angle $\text{C}(1)-\text{C}(6)/\text{O}(13)-\text{H}(14)$ at different dihedral angles of $\text{C}(4)-\text{C}(3)/\text{S}(11)-\text{H}(12)$ from 0 to 90° . (C) The vibrational cross-angle difference Er vs the $\text{C}(4)-\text{C}(3)/\text{S}(11)-\text{H}(12)$ dihedral angle at a fixed $\text{C}(1)-\text{C}(6)/\text{O}(13)-\text{H}(14)$ dihedral angle 0° . The variation is only $\sim 0.2^\circ$, substantially smaller than the experimental uncertainty $\sim 1^\circ$. The DFT calculations were performed using the CPCM model in CCl_4 with B3LYP/6-311++G(d,p).

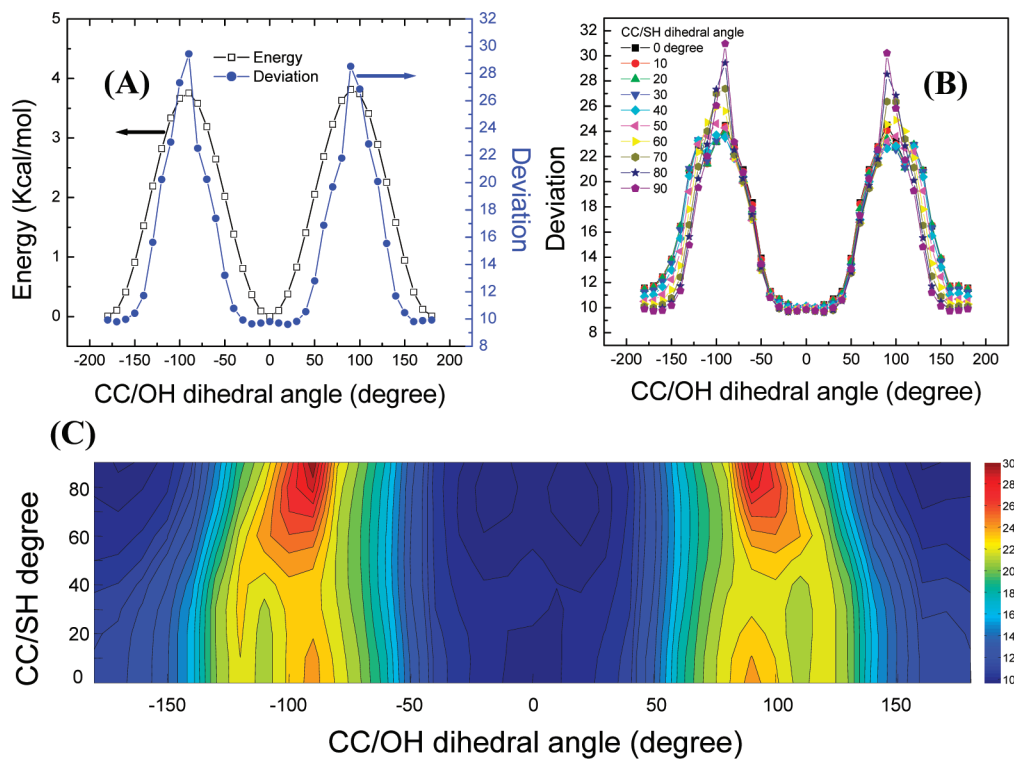


Figure 7. (A) Calculated potential energy surface of hydrogen-bonded 4-mercaptophenol (left axis) and the difference between calculated and experimental vibrational cross-angles Er vs the CC/OH dihedral angle $\text{C}(1)-\text{C}(6)/\text{O}(13)-\text{H}(14)$ (right axis), with a fixed dihedral angle of $\text{C}(4)-\text{C}(3)/\text{S}(11)-\text{H}(12)$ $\text{C}(4)-\text{C}(3)/\text{S}(11)-\text{H}(12)$ at -83° (the calculated optimal angle). (B) Vibrational cross-angle difference Er vs the CC/OH dihedral angle $\text{C}(1)-\text{C}(6)/\text{O}(13)-\text{H}(14)$ at different dihedral angles of $\text{C}(4)-\text{C}(3)/\text{S}(11)-\text{H}(12)$ from 0 to 90° . (C) The two-dimensional vibrational angle difference Er along the $\text{C}(1)-\text{C}(6)/\text{O}(13)-\text{H}(14)$ and $\text{C}(4)-\text{C}(3)/\text{S}(11)-\text{H}(12)$ dihedral angles of the polycrystalline sample. Similar to the CCl_4 solution sample, the most stable conformation of this molecule in its crystal also has its OH group almost coplanar to the benzene ring. The level and basis used for the calculation is B3LYP/6-311++G(d,p). Each contour represents 4% amplitude change, while when the deviation Er is lower than 10 , each contour represents 0.8% change.

along these two rotational degrees of freedom [along the $\text{C}(1)-\text{C}(6)/\text{O}(13)-\text{H}(14)$ and $\text{C}(4)-\text{C}(3)/\text{S}(11)-\text{H}(12)$ dihedral angles], DFT calculations show that in the most stable conformation, the dihedral angle of $\text{C}(1)-\text{C}(6)/\text{O}(13)-\text{H}(14)$ is 0.3° (0° within calculation error), and the dihedral angle of $\text{C}(4)-\text{C}(3)/\text{S}(11)-\text{H}(12)$ is -72° . The conformation is displayed in Figure 5B. The potential surface and the experimental and calculated vibrational angle difference Er of molecular conformations rotating along the C–O single bond

with a fixed $\text{C}(4)-\text{C}(3)/\text{S}(11)-\text{H}(12)$ dihedral angle -72° in Figure 5A are strikingly similar. Both show that for the isolated molecule, the OH group is coplanar to the benzene ring in the most probable conformation. In addition, for the molecule in CCl_4 solution, the vibrational angle difference values in the range of the $\text{C}(1)-\text{C}(6)/\text{O}(13)-\text{H}(14)$ dihedral angle from -20 to 20° are very close (within 0.2° difference). They are all within experimental uncertainty (about 1°). The result suggests that populations of conformations within this range are

substantial. This is consistent with the calculated potential surface where the energy of the conformation with OH 20° out of the ring plane is only about 0.3 kcal/mol higher than that of the most stable conformation. At room temperature (295 K), the population of this conformation is $\sim e^{-0.3/0.6} = 61\%$ of that of the most stable one.

The S–H group rotating around the C–S bond also generates a potential surface (in Figure 6A) similar to that from OH rotating along the O–C bond. However, this potential surface is much flatter. The difference between the energy minimum and the maximum is only 0.22 kcal/mol, which means that at room temperature (295 K), the population of the least probable conformation is still quite substantial. It is $\sim e^{-0.22/0.6} = 69\%$ of the population of the most probable conformation. In other words, at room temperature, the probability of the S–H group assuming any angle relative to the benzene ring is comparable. Experimental data show a similar result. As Figure 6B,C displays, S–H rotating along the C–S for 90° only change $\Delta\theta \sim 0.2^\circ$. In addition, at any C(4)–C(3)/S(11)–H(12) dihedral angle, the O–H group is always coplanar to the benzene ring, as predicted by calculations and measured with experiments (Figure 6B). The experimental 2D IR data, detailed vibrational cross-angles, and calculations with different levels are provided in the Supporting Information.

3.4.2. Molecular Conformation of 4-Mercaptophenol Crystal. In the 4-mercaptophenol crystal, most OH groups form hydrogen bonds, as shown in Figure 2B, where the free OH peak in the CCl_4 solution disappears and a broad OH band between 3000 to 3600 cm^{-1} appears. The hydrogen bonds are expected to distort the molecular conformation by dragging the OH group out of the benzene plane for a few degrees, as XRD data of crystalline phenol show that the hydrogen bonds among phenol molecules on average distort the OH group $\sim 6^\circ$ away from the benzene plane.⁶²

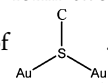
The vibrational angle calculations for the crystalline sample are different from those for the CCl_4 solution. In the crystalline samples, the OH groups are hydrogen bonded. It is well-known that hydrogen bonds can severely reduce the vibrational lifetimes of the hydroxyl stretch mode from tens or hundreds ps to a few ps.^{20,53} To account for the effect of hydrogen bonds on vibrational couplings, we used the optimized structure of a hydrogen-bonded 4-mercaptophenol rather than an isolated molecule to calculate the vibrational cross-angles. In the vibrational cross-angle calculations, the hydrogen bond partner of this hydrogen-bonded 4-mercaptophenol was taken away to avoid mixing vibrational vectors. Calculations using an isolated molecule were also performed, giving essentially the same results as the new method. Both calculated and experimental data are provided in the Supporting Information.

Experimental vibrational cross-angle measurements on the polycrystalline 4-mercaptophenol sample give a very similar molecular conformation to that in the CCl_4 dilute solution. In Figure 7A, the vibrational angle difference between experimental and calculated values has a minimum when the OH group is 20° out of the benzene ring. However, the angle difference values at C(1)–C(6)/O(13)–H(14) dihedral angles -30 – 30° are very similar ($\sim 0.2^\circ$). This suggests that most of the OH groups in the crystal reside within 30° of the benzene plane rather than dominantly at 20°. Similar to the CCl_4 solution, the S–H group can assume almost any angle relative to the ring plane. At any of these angles, the OH group are always within 30° of the benzene plane, as manifested by the two-dimensional vibrational angle difference along the C(1)–

C(6)/O(13)–H(14) and C(4)–C(3)/S(11)–H(12) dihedral angles in Figure 7B,C.

In Figure 7A, the CC/OH dihedral angle has a broad minimum, similar to the molecules in solution. This result seems surprising, since one would expect that the ordering of the crystal would cause a more rigid molecular structure than in the liquid phase. There are a few plausible reasons. The width of the minimum is determined by the relative energy of the conformations with different dihedral angles. Because the relative energy is mainly determined by how far the OH is distorted away from the ring plane, the width is mainly determined by the intramolecular structure rather than the intermolecular interaction. This implies that in the crystal, the molecules or chemical bonds have certain degrees of freedom to rotate (or wobble). This turns out to be true. The molecular crystal can be regarded as a plastic crystal. According to the definition of plastic crystals, the molecules inside a plastic crystal are wobbling.⁶³ The wobbling is not necessarily slower than its rotation in liquids! For instance, as we have measured,¹⁷ in the KSCN crystal, the rotational time constant of SCN is ~ 11 ps, same as in its concentrated aqueous solution! Certainly in crystal, the rotation is hindered. It can only wobble for $\sim 30^\circ$.

3.4.3. Molecular Conformation of 4-Mercaptophenol on the Gold Nanoparticle Surface. On the surfaces of gold nanoparticles, the ligand thiol molecules are known to form covalent S–Au bonds with the particles.^{64–66} In particular, recent XRD data show that on a gold nanoparticle, the ligand molecules are closely packed on the surface with coverage around 70%, and all thiol molecules actually form two S–Au bonds with the particles in the bridge form of



¹⁸ The locations of these S–Au bonds and the arrangement of surface Au atoms inevitably impose geometric constraints on the intermolecular interactions of the ligand molecules and therefore affect their conformations. For the model system studied here, 4-mercaptophenol coated on 3.5 nm Au nanoparticles, our FTIR measurements (Figure 2) have suggested the formations of S–Au bonds between the molecule and the particle and hydrogen bonds among the OH groups of the molecules on the particle surfaces. The hydrogen bonds of these surface molecules are expected not to be the same as those energy-optimized in the molecular crystal, as the formation of these surface hydrogen bonds is affected by the geometric constraints imposed by the adsorption. To form a hydrogen bond with a neighbor molecule, the OH group of one 4-mercaptophenol molecule might be expected to rotate for a certain angle to compensate for the spatial mismatch. This angle distortion cannot be predicted by DFT calculations because there is no detailed information about where the ligand molecules reside with respect to the surface Au atoms. The vibrational cross-angle measurements for determining molecular conformations in liquid and solid presented in the above are able to address this problem.

Similar to the experiments for the 4-mercaptophenol solution and crystal samples, the vibrational cross-angles among the same 16 pairs of normal modes of the surface 4-mercaptophenol molecules on the 3.5 nm Au nanoparticles were determined. The experimental results (Figures 8 and 9) show that different from the liquid or crystalline samples where the OH group is about coplanar to the benzene ring, on the nanoparticle surfaces, the OH group is about 50–60° out of the

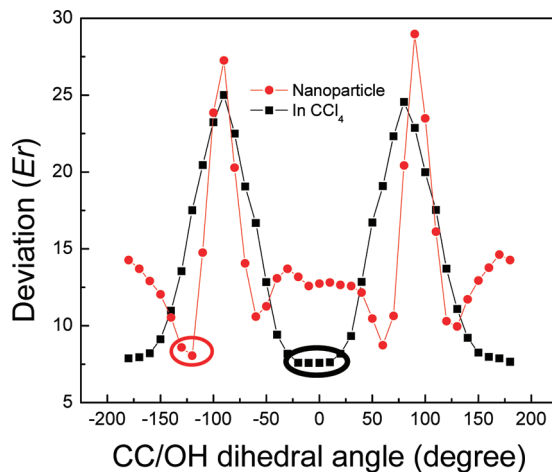


Figure 8. Vibrational cross-angle difference E_r vs the CC/OH dihedral angle of the 4-mercaptophenol in the CCl_4 solution and the coated gold nanoparticle sample. The CC/S_H dihedral angles of both samples were fixed at different angles to reach the global minimum, -72° for the solution and 10° (β , defined in Figure 9A) for the particle sample.

benzene plane. The global and local minimal vibrational angle difference values always occur when OH is $\sim 60 \pm 10^\circ$ out of the benzene plane (the CC/OH dihedral angle is $60, 160, -20$, and -120°), regardless how the molecule rotates around the C–S single bond, as demonstrated in Figure 9B. Here, we want to point out one issue. Because our data are ensemble results, although the minima along the CC/OH dihedral angle are sharper than the minimum in the solution, they cannot be considered as an indication of an ordered, homogeneous molecular distribution on the gold surface.

The results (Figure 9B) show that on the nanoparticle surfaces, the OH group is about $50\text{--}60^\circ$ out of the benzene plane, and one S–Au bond is $\sim 20^\circ$ out of the benzene ring. The Au–S–Au angle was determined to be 110° (see the Supporting Information). With these angles determined, the most probable average three-dimensional molecular conformation of 4-mercaptophenol on the 3.5 nm Au nanoparticles is readily constructed, shown in Figure 9A. During the construction of the 3D conformations, we utilized our

experimental results (the collective surface electronic motion does not affect the ligand molecule's intramolecular vibrational couplings) of the vibrational dynamics measurements on the particle surfaces to simplify the calculations for vibrational cross-angles by reducing the number of gold atoms of the nanoparticles into a cluster of two Au atoms.

The distortion of the OH group about $50\text{--}60^\circ$ away from the conjugation plane of 4-mercaptophenol on the particle surface (Figure 8) is significantly different from the calculated energy-optimized structure (OH coplanar to the ring, in SM) without considering the Au atomic array or the detailed S–Au binding locations on the particle surface. As described above, this is probably the balanced result of the surface geometric constraint, $\pi\text{--}\pi$ stacking, and hydrophobic interactions on the formation of hydrogen bonds among the surface OH groups. The 4-mercaptophenol molecule has two ways to overcome the geometric constraint to form a hydrogen bond with a neighbor molecule: one is to rotate along the C–O single bond, and the other is to rotate along the C–S single bond. DFT calculations for isolated molecules show that rotating the OH group $50\text{--}60^\circ$ away from the conjugation plane increases the system energy about 2–2.7 kcal/mol (still much more stable than the nonbonded species), as compared to the most stable coplanar conformation. Rotating about the C–S bond must cross a barrier about 1.4–2 kcal/mol (in the Supporting Information). The two barriers are close, suggesting that both rotations are energetically possible. However, the rotation around the C–S bond involves the motion of the bulky benzene ring, which can substantially change the $\pi\text{--}\pi$ stacking (and possibly other intermolecular interactions) in the real system. This issue was not considered in the calculations. The change of $\pi\text{--}\pi$ stacking can significantly increase the system energy. Therefore, from the energy point of view, rotating along the C–O bond to form a hydrogen bond with the OH groups of another surface 4-mercaptophenol molecule is probably more favorable. The experimental results suggest that, even for a very simple molecule as 4-mercaptophenol studied here, without the detailed knowledge about surface properties of a nanoparticle, the calculated energy-optimized molecular conformations on the particle surface can be substantially different from the real situation.

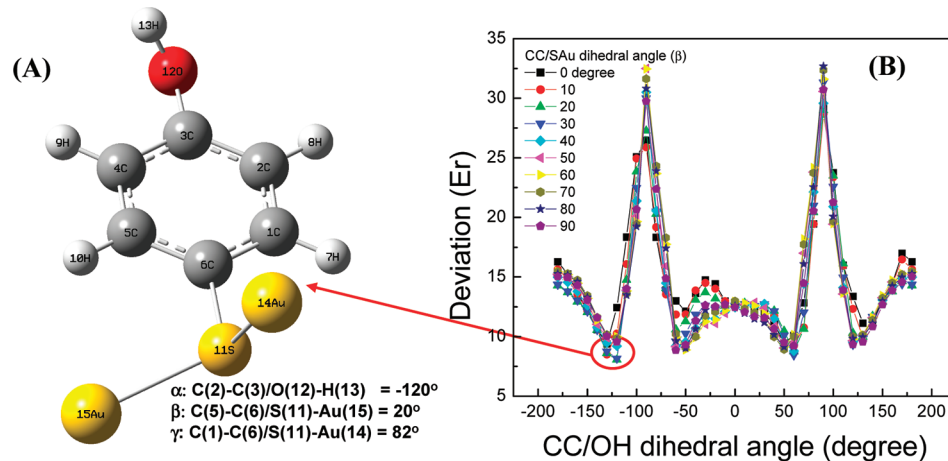


Figure 9. (A) Most probable conformation of $\text{HOC}_6\text{H}_4\text{--S(Au)}_2$ on the surface of 3.5 nm Au nanoparticle determined by experiments. α , β , and γ are the dihedral angles as defined. (B) Experimental and calculated vibrational cross-angle deviation E_r vs the CC/OH dihedral angle $\text{C}(2)\text{--C}(3)/\text{O}(12)\text{--H}(13)$ at different dihedral angles of $\text{C}(5)\text{--C}(6)/\text{S}(11)\text{--Au}(15)$ (β) from 0 to 90° . The calculation level used for the gold atom is B3LYP/LanL2DZ, and B3LYP/6-311++G(d,p) is for other atoms. E_r reaches the global minimum when $\alpha = -120^\circ$ and $\beta = 20^\circ$.

4. CONCLUDING REMARKS

In this work, the three-dimensional molecular conformations and vibrational dynamics of a model compound, 4-mercaptophenol, on the surface of 3.5 nm gold nanoparticles were investigated with an ultrafast multiple-mode multiple-dimensional infrared spectroscopic technique. It was found that on the particle surface, the ligand molecules cannot form energy-optimized hydrogen bonds mainly because of a surface geometry constraint. The observation is supported by comparison with the structures of the ligand molecule in the crystal phase and in a dilute CCl_4 solution. This capability of resolving 3D molecular conformations on nanomaterials surfaces is expected to be helpful for understanding specific intermolecular interactions and conformation-selective reactions (e.g., chirality selectivity) on the surfaces of these materials. Our experiments also showed that the effect of the particle surface nonadiabatic electron/vibration coupling does not play a significant role in the vibrational relaxation of high frequency modes ($>1000 \text{ cm}^{-1}$) of the ligand molecules about 3 Å away from the nanoparticle surface. Simple theoretical calculations support the observation. With the extension of the laser frequencies down to 100 cm^{-1} or lower, we expect that not only the surface molecular conformations but also the direct interactions involving the S–Au bonds between the surface molecule and the particle can be directly probed by the method. Regarding the generality of our approach in resolving 3D molecular conformations, we want to discuss a key issue here. So far, the molecules of which conformations determined by our approach are relatively small. They do not have any vibrational spectral overlap issue. This problem may become very serious if the molecules are big, for example, proteins or DNAs. To address this problem, we propose two approaches, which are undergoing in our lab: (1) to accumulate a database for building blocks of big molecules. The structure of the molecule will be constructed based on the signal assembly from the building blocks. This approach has a requirement: modes studied should be mainly localized within a few chemical bonds; and (2) to expand the frequency range down to T-Herz, where many conformation-related modes reside.

■ ASSOCIATED CONTENT

Supporting Information

Supporting tables, figures, cross-angle measurements, vibrational time constant measurements, and detailed DFT calculations. This material is available free of charge via the Internet at <http://pubs.acs.org>.

■ AUTHOR INFORMATION

Corresponding Author

*E-mail: junrong@rice.edu.

Notes

The authors declare no competing financial interest.

■ ACKNOWLEDGMENTS

This material is based upon work supported by the Air Force Office of Scientific Research under AFOSR Award No. FA9550-11-1-0070 and the Welch foundation under Award No. C-1752. J.Z. also thanks the David and Lucile Packard Foundation for a Packard fellowship. We also thank Prof. Robert Curl's substantial discussions and suggestions and language modifications of the manuscript and Dr. Hongjun Fan's insightful discussion about DFT calculations.

■ REFERENCES

- (1) Murray, C. B.; Kagan, C. R.; Bawendi, M. G. *Annu. Rev. Mater. Sci.* **2000**, *30*, 545.
- (2) Penn, S. G.; He, L.; Natan, M. J. *Curr. Opin. Chem. Biol.* **2003**, *7*, 609.
- (3) Bell, A. T. *Science* **2003**, *299*, 1688.
- (4) Park, S. J.; Taton, T. A.; Mirkin, C. A. *Science* **2002**, *295*, 1503.
- (5) Sperling, R. A.; River agil, P.; Zhang, F.; Zanella, M.; Parak, W. J. *Chem. Soc. Rev.* **2008**, *37*, 1896.
- (6) Maxwell, D. J.; Taylor, J. R.; Nie, S. M. *J. Am. Chem. Soc.* **2002**, *124*, 9606.
- (7) Ghosh, A.; Smits, M.; Bredenbeck, J.; Dijkhuizen, N.; Bonn, M. *Rev. Sci. Instrum.* **2008**, *79*, 9.
- (8) Huang, X. H.; Jain, P. K.; El-Sayed, I. H.; El-Sayed, M. A. *Nanomedicine* **2007**, *2*, 681.
- (9) Shukla, N.; Bartel, M. A.; Gellman, A. J. *J. Am. Chem. Soc.* **2010**, *132*, 8575.
- (10) Pissuwan, D.; Valenzuela, S. M.; Cortie, M. B. *Trends Biotechnol.* **2006**, *24*, 62.
- (11) Wu, Z. W.; Gayathri, C.; Gil, R. R.; Jin, R. C. *J. Am. Chem. Soc.* **2009**, *131*, 6535.
- (12) Bian, H. T.; Li, J. B.; Wen, X. W.; Sun, Z. G.; Song, J.; Zhuang, W.; Zheng, J. R. *J. Phys. Chem. A* **2011**, *115*, 3357.
- (13) Jin, Q.; Rodriguez, J. A.; Li, C. Z.; Darici, Y.; Tao, N. J. *Surf. Sci.* **1999**, *425*, 101.
- (14) Bian, H.; Li, J.; Wen, X.; Zheng, J. R. *J. Chem. Phys.* **2010**, *132*, 184505.
- (15) Bian, H. T.; Wen, X. W.; Li, J. B.; Zheng, J. R. *J. Chem. Phys.* **2010**, *133*, 034505.
- (16) Bian, H. T.; Wen, X. W.; Li, J. B.; Chen, H. L.; Han, S.; Sun, X. Q.; Song, J.; Zhuang, W.; Zheng, J. R. *Proc. Natl. Acad. Sci.* **2011**, *108*, 4737.
- (17) Bian, H. T.; Chen, H. L.; Li, J. B.; Wen, X. W.; Zheng, J. R. *J. Phys. Chem. A* **2011**, *115*, 11657.
- (18) Jadzinsky, P. D.; Calero, G.; Ackerson, C. J.; Bushnell, D. A.; Kornberg, R. D. *Science* **2007**, *318*, 430.
- (19) Gaffney, K. J.; Piletic, I. R.; Fayer, M. D. *J. Chem. Phys.* **2003**, *118*, 2270.
- (20) Zheng, J.; Fayer, M. D. *J. Phys. Chem. B* **2008**, *112*, 10221.
- (21) Fermi, E. *Z. Phys.* **1931**, *71*, 250.
- (22) Wilson, E. B., Jr.; Decius, J. C.; Cross, P. C. *Molecular Vibrations: The Theory of Infrared and Raman Vibrational Spectra*; McGraw-Hill: New York, 1955.
- (23) Zheng, J.; Kwak, K.; Steinle, T.; Asbury, J. B.; Chen, X.; Xie, J.; Fayer, M. D. *J. Chem. Phys.* **2005**, *123*, 164301.
- (24) Khalil, M.; Demirdoven, N.; Tokmakoff, A. *J. Phys. Chem. A* **2003**, *107*, 5258.
- (25) Peng, C. S.; Jones, K. C.; Tokmakoff, A. *J. Am. Chem. Soc.* **2011**, *133*, 15650.
- (26) Kornau, K. M.; Rickard, M. A.; Mathew, N. A.; Pakoulev, A. V.; Wright, J. C. *J. Phys. Chem. A* **2011**, *115*, 4054.
- (27) Rubtsov, I. V.; Kumar, K.; Hochstrasser, R. M. *Chem. Phys. Lett.* **2005**, *402*, 439.
- (28) Woutersen, S.; Hamm, P. *J. Phys. Chem. B* **2000**, *104*, 11316.
- (29) Zanni, M. T.; Gnanakaran, S.; Stenger, J.; Hochstrasser, R. M. *J. Phys. Chem. B* **2001**, *105*, 6520.
- (30) Hahn, S.; Lee, H.; Cho, M. *J. Chem. Phys.* **2004**, *121*, 1849.
- (31) Maekawa, H.; De Poli, M.; Moretto, A.; Toniolo, C.; Ge, N. H. *J. Phys. Chem. B* **2009**, *113*, 11775.
- (32) Rubtsov, I. V. *Acc. Chem. Res.* **2009**, *42*, 1385.
- (33) Baiz, C. R.; McRobbie, P. L.; Anna, J. M.; Geva, E.; Kubarych, K. *J. Acc. Chem. Res.* **2009**, *42*, 1395.
- (34) Nydegger, M. W.; Dutta, S.; Cheatum, C. M. *J. Chem. Phys.* **2010**, *133*, 8.
- (35) Shim, S. H.; Strasfeld, D. B.; Ling, Y. L.; Zanni, M. T. *Proc. Natl. Acad. Sci. U.S.A.* **2007**, *104*, 14197.
- (36) Zhuang, W.; Abrarnavicius, D.; Voronine, D. V.; Mukarmel, S. *Proc. Natl. Acad. Sci. U.S.A.* **2007**, *104*, 14233.

- (37) Cahoon, J. F.; Sawyer, K. R.; Schlegel, J. P.; Harris, C. B. *Science* **2008**, *319*, 1820.
- (38) Zheng, J.; Kwac, K.; Xie, J.; Fayer, M. D. *Science* **2006**, *313*, 1951.
- (39) Kumar, K.; Sinks, L. E.; Wang, J. P.; Kim, Y. S.; Hochstrasser, R. M. *Chem. Phys. Lett.* **2006**, *432*, 122.
- (40) Xu, C.; Lai, X.; Zajac, G. W.; Goodman, D. W. *Phys. Rev. B* **1997**, *S6*, 13464.
- (41) Valden, M.; Lai, X.; Goodman, D. W. *Science* **1998**, *281*, 1647.
- (42) Chen, M. S.; Goodman, D. W. *Science* **2004**, *306*, 252.
- (43) Paulus, P. M.; Goossens, A.; Thiel, R. C.; van der Kraan, A. M.; Schmid, G.; de Jongh, L. *J. Phys. Rev. B* **2001**, *64*, 18.
- (44) Daniel, M. C.; Astruc, D. *Chem. Rev.* **2004**, *104*, 293.
- (45) Wodtke, A. M.; Tully, J. C.; Auerbach, D. *J. Int. Rev. Phys. Chem.* **2004**, *23*, 513.
- (46) Nahler, N. H.; White, J. D.; Larue, J.; Auerbach, D. J.; Wodtke, A. M. *Science* **2008**, *321*, 1191.
- (47) Nordlander, P.; Tully, J. C. *Phys. Rev. B* **1990**, *42*, 5564.
- (48) Beckerle, J. D.; Cavanagh, R. R.; Casassa, M. P.; Heilweil, E. J.; Stephenson, J. C. *J. Chem. Phys.* **1991**, *95*, 5403.
- (49) Tully, J. C. *Annu. Rev. Phys. Chem.* **1980**, *31*, 319.
- (50) Morin, M.; Levinos, N. J.; Harris, A. L. *J. Chem. Phys.* **1992**, *96*, 3950.
- (51) Andersson, S.; Pendry, J. B. *Phys. Rev. Lett.* **1979**, *43*, 363.
- (52) Persson, B. N. J.; Persson, M. *Solid State Commun.* **1980**, *36*, 175.
- (53) Zheng, J. R.; Fayer, M. D. *J. Am. Chem. Soc.* **2007**, *129*, 4328.
- (54) Ekardt, W.; Penzar, Z. *Phys. Rev. B* **1986**, *34*, 8444.
- (55) Corni, S.; Tomasi, J. *J. Chem. Phys.* **2001**, *114*, 3739.
- (56) Blaber, M. G.; Arnold, M. D.; Ford, M. J. *J. Phys. Chem. C* **2009**, *113*, 3041.
- (57) Liebsch, A. *Phys. Rev. Lett.* **1985**, *54*, 67.
- (58) Lampert, H.; Mikenda, W.; Karpfen, A. *J. Phys. Chem. A* **1997**, *101*, 2254.
- (59) Headgordon, M.; Pople, J. A. *J. Phys. Chem.* **1993**, *97*, 1147.
- (60) Pedersen, T.; Larsen, N. W.; Nygaard, L. *J. Mol. Struct.* **1969**, *4*, 59.
- (61) Larsen, N. W.; Nicolais, F. *J. Mol. Struct.* **1974**, *22*, 29.
- (62) Zavodnik, V. E.; Belskii, V. K.; Zorkii, P. M. *J. Struct. Chem.* **1987**, *28*, 793.
- (63) Timmermans, J. *J. Phys. Chem. Solids* **1961**, *18*, 1.
- (64) Brust, M.; Fink, J.; Bethell, D.; Schiffri, D. J.; Kiely, C. *J. Chem. Soc.-Chem. Commun.* **1995**, 1655.
- (65) Chen, S. W. *Langmuir* **1999**, *15*, 7551.
- (66) Stolarczyk, K.; Palys, B.; Bilewicz, R. *J. Electroanal. Chem.* **2004**, *564*, 93.

**Molecular conformations and dynamics on surfaces of gold
nanoparticles probed with multiple-mode multiple-dimensional infrared
spectroscopy**

Hongtao Bian, Jiebo Li, Hailong Chen, Kaijun Yuan, Xiewen Wen, Yaqin Li, Zhigang Sun, Junrong Zheng^{*}

* To whom correspondence should be addressed. E-mail: junrong@rice.edu

Supporting materials

This file includes:

Supporting material text

Figure S1 to S12

Table S1 to S4

References

Table S1. Scaling factors for the 2D IR spectrum of 4-Mercaptophenol on the surfaces of 3.5nm Au nanoparticles.

Probe frequency Region	Pump frequency region	Scaling factor (×)
Probe 1130-1300 cm ⁻¹	1100-1400 & 3000-3720 cm ⁻¹	3.0
Probe 1130-1300 cm ⁻¹	1400-1700 cm ⁻¹	6.0
Probe 1390-1440 cm ⁻¹	1100-3720 cm ⁻¹	5.0
Probe 1455-1510 cm ⁻¹	1100-3720 cm ⁻¹	1.0
Probe 1555-1620 cm ⁻¹	1100-3720 cm ⁻¹	2.0
Probe 3000-3400 cm ⁻¹	1100-3720 cm ⁻¹	2.0

Mathematical analysis of the effects of Fermi resonances on vibrational transition dipole directions

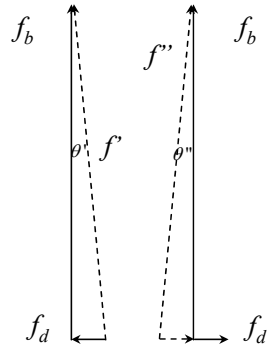


Figure S1. Vector diagrams representing the change of transition dipole directions as a result of Fermi resonance. f_b and f_d indicates the oscillator strengths of bright mode and dark mode respectively.

The Hamiltonian of a Fermi resonance between two oscillators can be described as

$$H = \omega_1 a_1^\dagger a_1 + \omega_2 a_2^\dagger a_2 + \frac{\Delta}{2} (a_1 a_2^{\dagger 2} + a_1^\dagger a_2),$$

where a_i^\dagger and a_i are the creation and annihilation operators of the two modes respectively, with the accidental resonance condition $\omega_1 \approx 2\omega_2$, and Δ represents the coupling between two modes. By diagonalizing the Hamiltonian in the basis $\{|1,0\rangle, |0,2\rangle\}$, and assuming $\omega_1 = 2\omega_2$, we could simply obtain the eigenenergies (I)

$$E_1 = \omega_1 - \frac{\Delta}{2},$$

$$E_2 = \omega_1 + \frac{\Delta}{2},$$

and the eigenstates

$$|\psi_1\rangle = +\frac{1}{\sqrt{2}}|1,0\rangle + \frac{1}{\sqrt{2}}|0,2\rangle,$$

$$|\psi_2\rangle = -\frac{1}{\sqrt{2}}|1,0\rangle + \frac{1}{\sqrt{2}}|0,2\rangle.$$

Therefore, the transition dipole moments become

$$\begin{aligned}\langle 0,0|\hat{\mu}|\psi_1\rangle &= \frac{1}{\sqrt{2}}(\langle 0,0|\hat{\mu}|1,0\rangle + \langle 0,0|\hat{\mu}|0,2\rangle) = \frac{1}{\sqrt{2}}(\boldsymbol{\mu}_b + \boldsymbol{\mu}_d), \\ \langle 0,0|\hat{\mu}|\psi_2\rangle &= \frac{1}{\sqrt{2}}(-\langle 0,0|\hat{\mu}|1,0\rangle + \langle 0,0|\hat{\mu}|0,2\rangle) = \frac{1}{\sqrt{2}}(-\boldsymbol{\mu}_b + \boldsymbol{\mu}_d).\end{aligned}$$

Usually, the value of transition dipole moment of the dark mode $|\boldsymbol{\mu}_d|$ is much smaller than that of the bright mode $|\boldsymbol{\mu}_b|$. When two states mix together, the oscillator strength of dark mode mainly gains from the bright one. Therefore, the transition dipole direction should be nearly the same as that of origin bright mode. For quantification, let $|\boldsymbol{\mu}_b| = 10|\boldsymbol{\mu}_d|$, and further assuming that the transition dipole moments of two modes are nearly perpendicular to each other, which will result in a maximum deviation. As shown in Fig. S1, the deviation of the direction can be easily calculated as $\theta \approx 5.7^\circ$. In most cases, the transition dipole moment ratio is much bigger than 10, resulting in $\theta < 1^\circ$.

Cross angle measurements

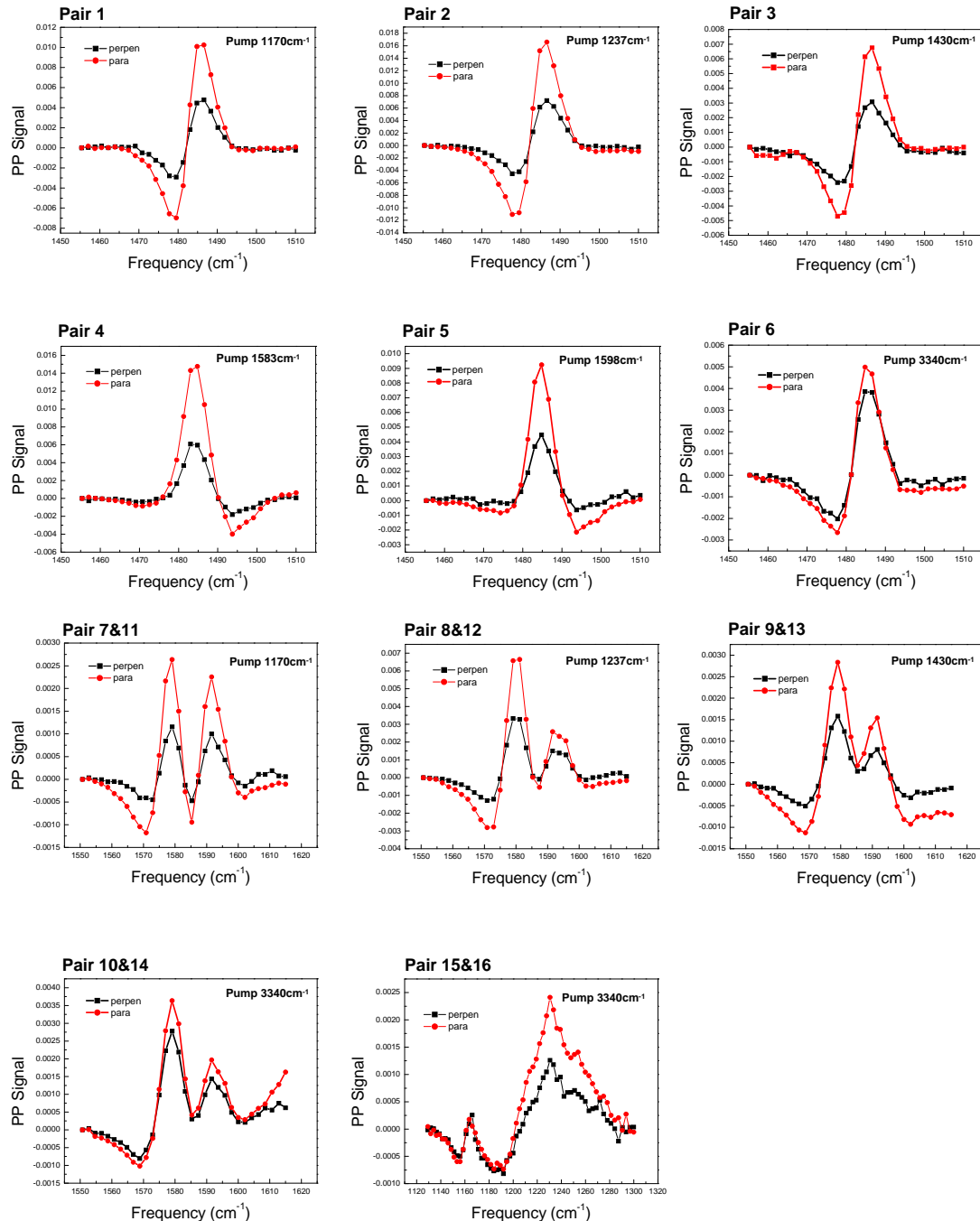


Fig. S2. Polarization selective pump probe data (parallel and perpendicular) for the 16 pair coupled modes of 4-mercaptophenol on the gold nanoparticle surface.

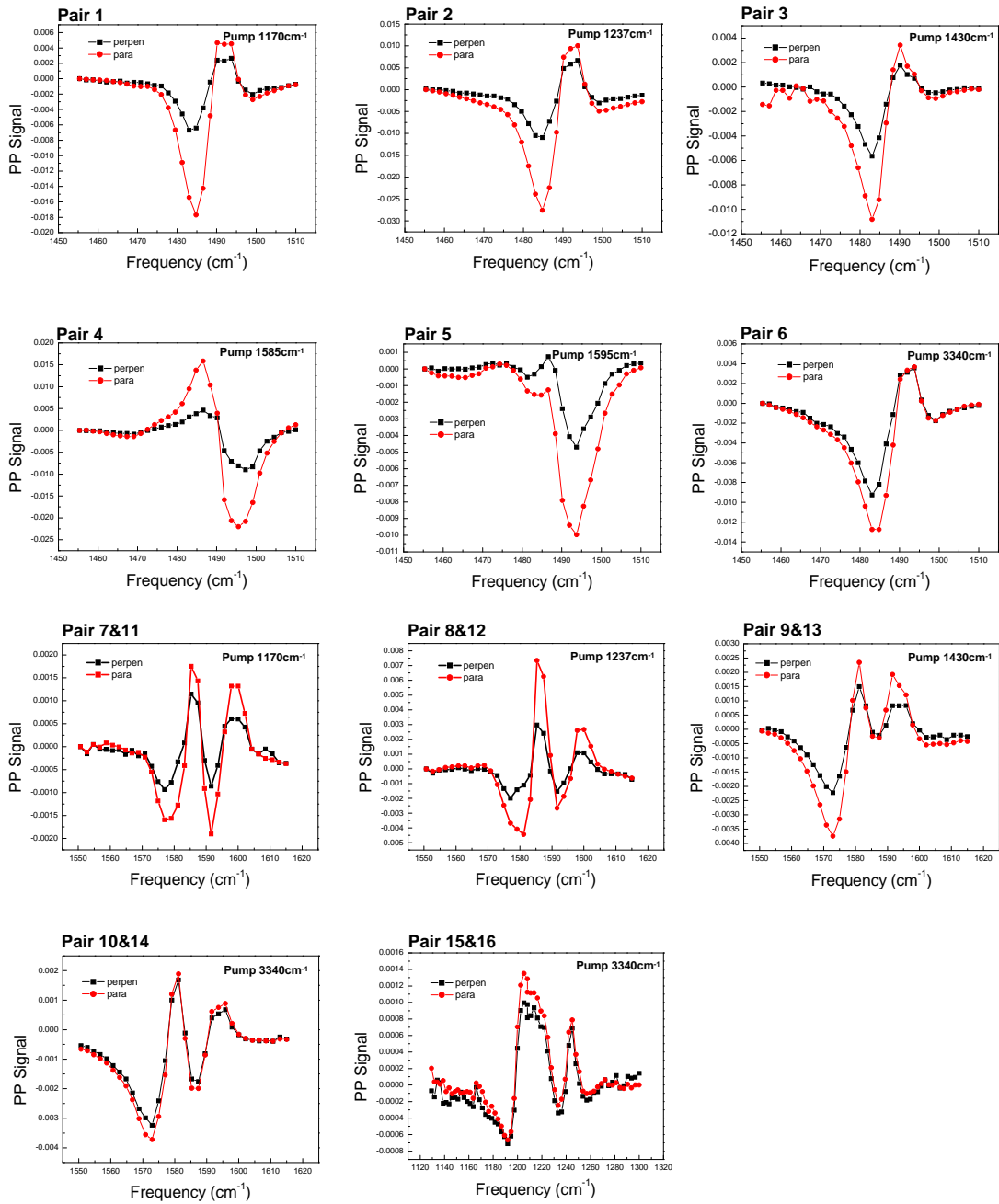


Fig. S3. Polarization selective pump probe data (parallel and perpendicular) for the 16 pair coupled modes of 4-mercaptophenol in the polycrystalline sample.

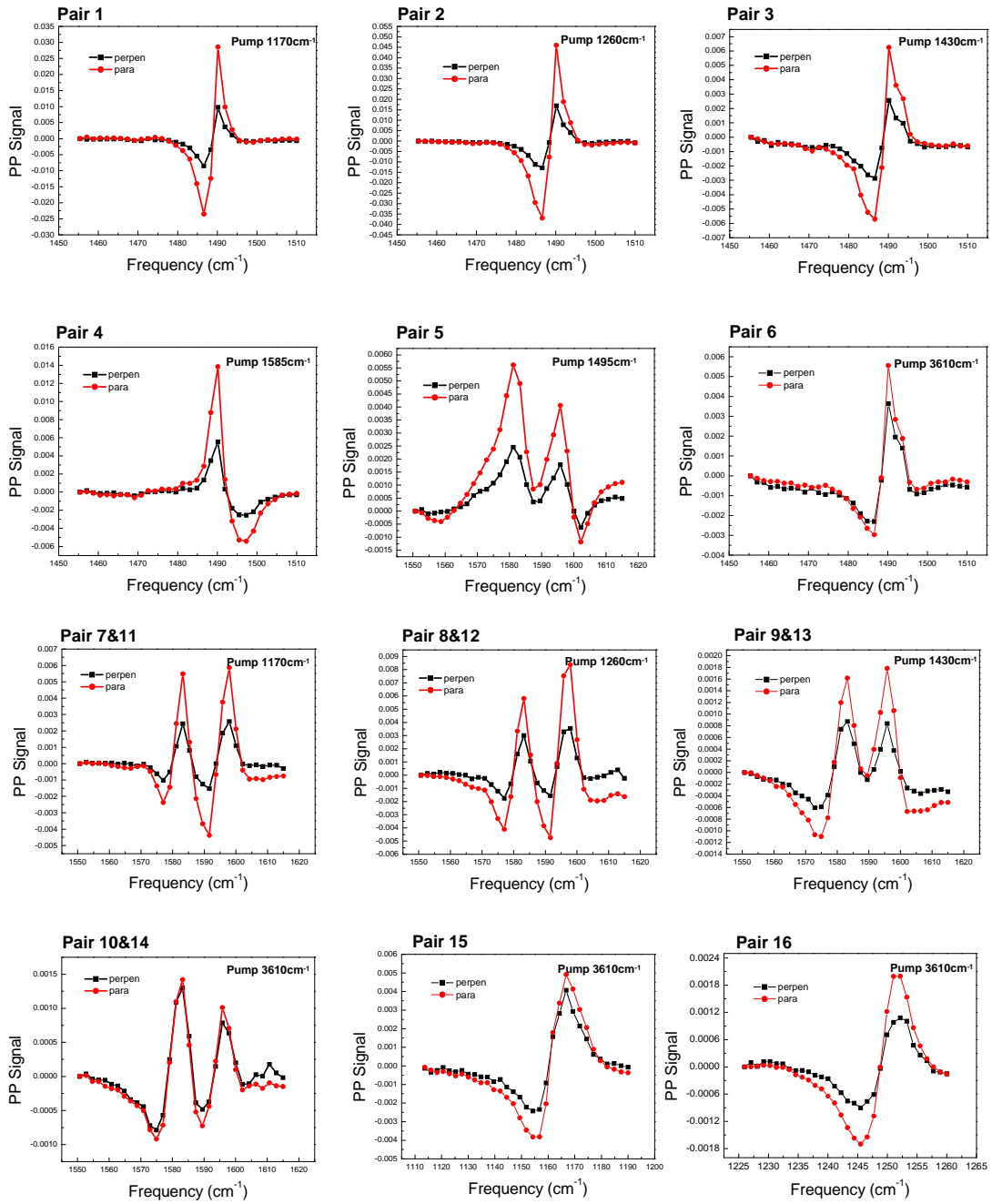


Fig. S4. Polarization selective pump probe data (parallel and perpendicular) for the 16 pair coupled modes of 4-mercaptophenol in the CCl_4 solution.

Vibrational time constant measurements

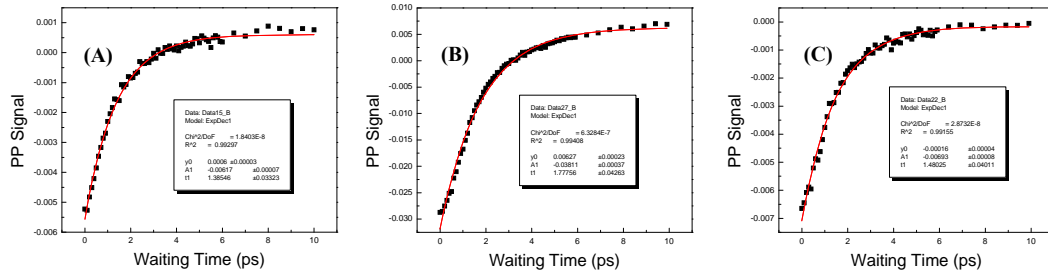


Fig. S5. Pump probe data for the O-H stretch mode (3340cm^{-1}) and fitting parameters for the vibrational lifetimes of 4-mercaptophenol in different environments (A) nanoparticle surface, (B) in polycrystalline sample and (C) in liquid CCl_4 .

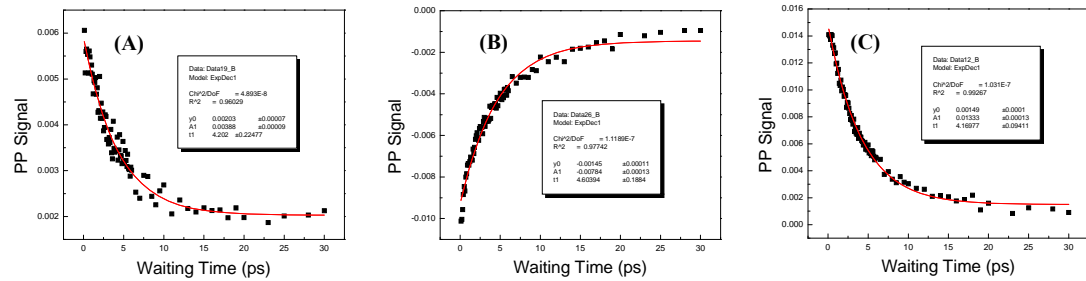


Fig. S6. Pump probe data for the C=C stretch mode (1584cm^{-1}) and fitting parameters for the vibrational lifetimes of 4-mercaptophenol in different environments (A) nanoparticle surface, (B) in polycrystalline sample and (C) in liquid CCl_4 .

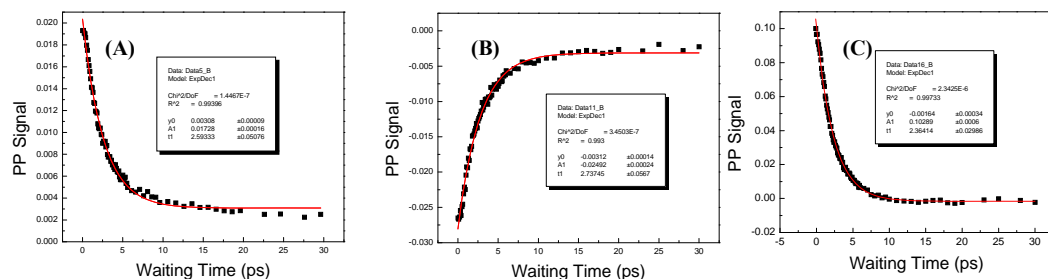


Fig. S7. Pump probe data for the C-C stretch mode (1488cm^{-1}) and fitting parameters for the vibrational lifetimes of 4-mercaptophenol in different environments (A) nanoparticle surface, (B) in polycrystalline sample and (C) in liquid CCl_4 .

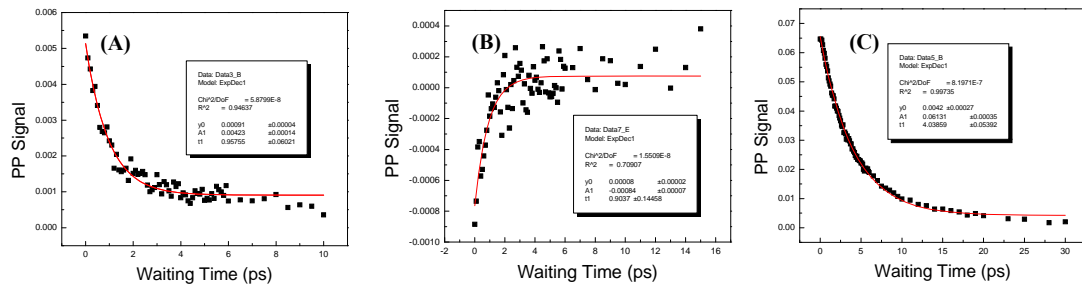


Fig. S8. Pump probe data for the C-O stretch mode (1237cm^{-1} or 1260 cm^{-1}) and fitting parameters for the vibrational lifetimes of 4-mercaptophenol in different environments (A) nanoparticle surface, (B) in polycrystalline sample and (C) in liquid CCl_4 .

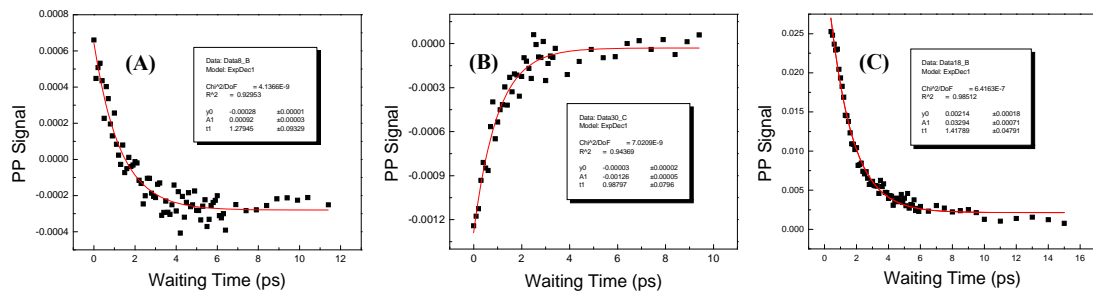


Fig. S9. Pump probe data for the OH bending mode (1170cm^{-1}) and fitting parameters for the vibrational lifetimes of 4-mercaptophenol in different environments (A) nanoparticle surface, (B) in polycrystalline sample and (C) in liquid CCl_4 .

Table S2. Calculated frequencies and assignments of 4-Mercaptophenol in the gas and in the CCl_4 solution. The level and basis used for the calculation is B3LYP/6-311++G(d,p). In CCl_4 solution, the SCRF-CPCM solvation model was used.

Normal modes	assignment	Experimental frequency (cm^{-1})			Calculated frequency (cm^{-1})	
		Gold nanoparticle	In polycrystalline sample	In CCl_4	In Gas	In CCl_4
22	O-H bending	1169	1170	1170	1187.45	1184.83
23	C-H scissoring	-	-	-	1192.72	1191.50
24	C-O stretch	1237	1237	1260	1280.50	1274.94
25	CH in plane rocking	-	-	-	1311.03	1311.95
26	CH in plane rocking+O-H bending	1350	1350	1320	1351.86	1351.08
27	CH in plane rocking+O-H bending	1430	1430	1420	1449.99	1447.54
28	C-H bending	1488	1495	1495	1522.90	1520.08
29	C=C stretch	1583	1586	1587	1621.19	1619.59
30	C=C stretch	1598	1599	1602	1637.87	1633.97
31	S-H stretch	-	2560	2588	2636.51	2646.40
32	C-H as	-	-	-	3153.46	3160.89
33	C-H as	-	-	-	3183.85	3182.62
34	C-H ss	-	-	-	3192.69	3192.80
35	C-H ss	-	-	-	3198.81	3197.29
36	OH stretch	3340	3340	3610	3834.31	3822.53

Table S3. *Transition dipole moment angles between coupled vibrational modes of the 4-mercaptophenol molecule on the gold nanoparticle surface, polycrystalline sample and CCl₄ solution. For comparison, the calculated cross angles of the isolated 4-mercaptophenol molecule at its optimized conformation were also listed. The level and basis used is B3LYP/6-311++G(d,p).*

Gold nanoparticle		polycrystalline sample		CCl ₄ solution		Calculation	
Coupled modes	Cross angle (degree)	Coupled modes	Cross angle (degree)	Coupled modes	Cross angle (degree)	Coupled modes	Cross angle (degree)
1169/1488	21±3	1170/1495	12±4	1169/1495	14±4	22/28	1.7
1237/1488	19±3	1237/1495	18±3	1260/1495	10±5	24/28	3.4
1430/1488	29±2	1430/1495	23±2	1430/1495	30±3	27/28	20.8
1583/1488	23±3	1586/1495	16±4	1583/1495	16±4	29/28	21.4
1598/1488	25±3	1599/1495	27±3	1598/1495	27±3	30/28	9.2
3340/1488	45±2	3340/1495	38±2	3610/1495	37±3	36/28	37.6
1169/1583	22±3	1170/1586	33±3	1170/1587	12±4	22/29	19.7
1237/1583	24±3	1237/1586	22±4	1260/1587	28±3	24/29	24.8
1430/1583	33±3	1430/1586	37±2	1430/1587	33±2	27/29	42.2
3340/1583	45±3	3340/1586	50±2	3610/1587	61±2	36/29	59.0
1169/1598	23±4	1170/1599	25±4	1170/1602	12±4	22/30	10.9
1237/1598	37±3	1237/1599	28±3	1260/1602	14±4	24/30	5.8
1430/1598	27±3	1430/1599	18±4	1430/1602	26±2	27/30	11.6
3340/1598	44±3	3340/1599	37±3	3610/1602	44±3	36/30	28.4
3340/1169	43±4	3340/1170	55±2	3610/1169	35±3	36/22	39.3
3340/1237	37±3	3340/1237	49±2	3610/1260	32±3	36/24	34.2

DFT calculations

The potential surfaces and calculated vibrational angles were obtained from density functional theory (DFT) calculations. The DFT calculations were carried out using Gaussian 09. Several levels and basis sets were used to compare the calculation results.

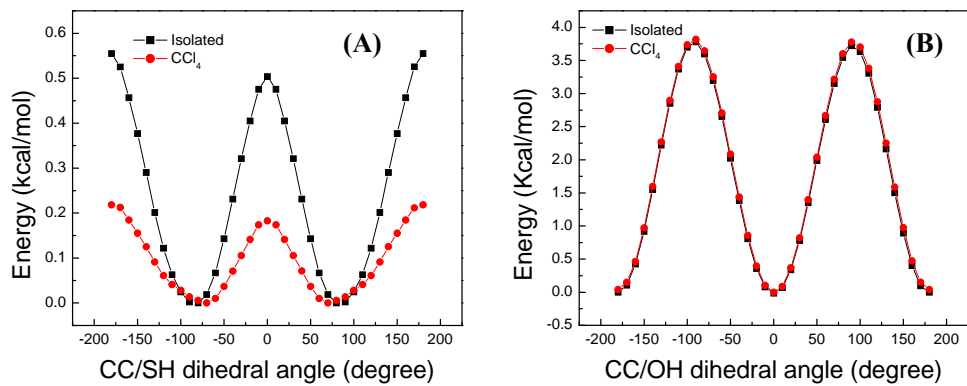


Fig. S10. Calculated potential energy surface (PES) of the 4-mercaptophenol in gas and in CCl_4 solution along (A) the CC/SH dihedral angle and (B) the CC/OH dihedral angle. The level and basis used for the calculation is B3LYP/6-311++G(d,p). The calculations indicate that the energy barrier for rotation along the C-S bond is very low.

DFT calculations for 4-mercaptophenol on the gold nanoparticle surfaces

The potential energy surface calculation of $\text{HOC}_6\text{H}_4\text{-SAu}_2$ molecule is displayed in Fig. S11. It indicates that the energy barrier for rotating the OH group 50~60 degrees away from the conjugation plane is about 2.0~2.7 kcal/mol, while rotating the Au-S bonds along the C-S bond must cross a barrier about 1.4~2.0 kcal/mol.

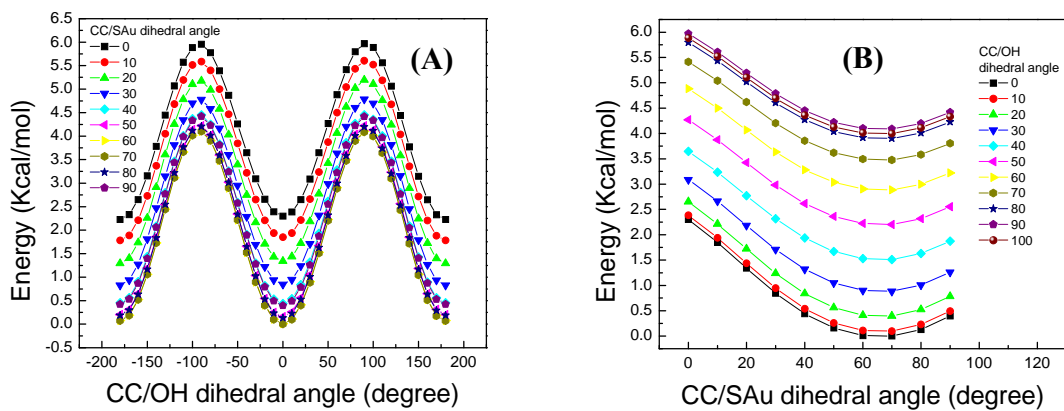


Fig. S11. (A) & (B) Calculated potential energy surface (PES) of the $\text{HOC}_6\text{H}_4\text{-SAu}_2$ molecule with varied CC/OH and CC/SAu dihedral angles. The level and basis used for the Au atoms is B3LYP/LanL2DZ. B3LYP/6-311++G(d,p) is for other atoms. The Au-S-Au angle is calculated to be ~126 degrees. The calculations show that the energy-optimized conformation is that with OH coplanar to the benzene ring, one S-Au bond 60 degrees out of the ring plane, and the Au-S-Au angle 126 degrees. This calculated conformation is similar to that of 4-mercaptophenol in the dilute CCl_4 solution but substantially different from the measured conformation on the particle surface, indicating that calculations without considering surface constraints can be quite off from the real situation.

In the DFT calculation of $\text{HOC}_6\text{H}_4\text{-SAu}_2$ molecule, the optimized Au-S-Au angle is 126 degrees. Previous XRD measurements(2) show that the Au-S-Au angles for a similar thiol are from 80 to 115 degrees. E_r data show that the most probable angle is 110 degrees (Fig.S12).

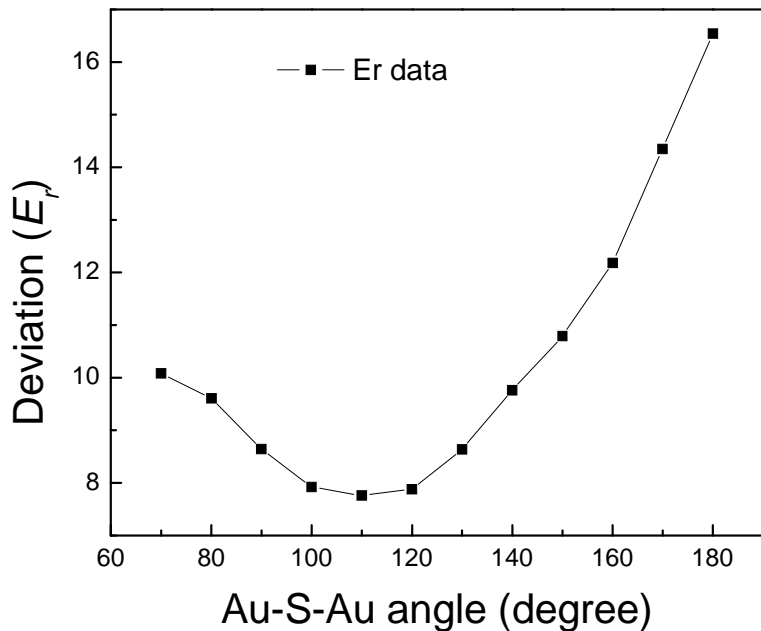


Fig. S12. E_r vs the Au-S-Au angle for the $\text{HOC}_6\text{H}_4\text{-SAu}_2$ molecule, the CC/OH dihedral angle was fixed at -120degree, while the CC/SAu dihedral angle was fixed at 20degree. The level and basis used for the Au atoms is B3LYP/LanL2DZ. B3LYP/6-311++G(d,p) is for other atoms. Calculations with angles smaller than 70 degrees couldn't be calculated probably because the two Au atoms are too close to each other under these small angles.

Reference

1. J. Edler, P. Hamm, *Journal of Chemical Physics* **119**, 2709 (Aug, 2003).
2. P. D. Jadzinsky, G. Calero, C. J. Ackerson, D. A. Bushnell, R. D. Kornberg, *Science* **318**, 430 (Oct, 2007).